DEVELOPMENT OF A WELL INTERVENTION TOOLKIT TO ANALYZE INITIAL WELLBORE CONDITIONS AND EVALUATE INJECTION PRESSURES, FLOW PATH, WELL KILL, AND PLUGGING PROCEDURES

A Dissertation

by

AMIR SAMAN PAKNEJAD

Submitted to the Office of Graduate Studies of
Texas A&M University
in partial fulfillment of the requirements for the degree of

DOCTOR OF PHILOSOPHY

August 2009

Major Subject: Petroleum Engineering

DEVELOPMENT OF A WELL INTERVENTION TOOLKIT TO ANALYZE INITIAL WELLBORE CONDITIONS AND EVALUATE INJECTION PRESSURES, FLOW PATH, WELL KILL, AND PLUGGING PROCEDURES

A Dissertation

by

AMIR SAMAN PAKNEJAD

Submitted to the Office of Graduate Studies of
Texas A&M University
in partial fulfillment of the requirements for the degree of

DOCTOR OF PHILOSOPHY

Approved by:

Chair of Committee,	Jerome Schubert
Committee Members,	Hans Juvkam-Wold
	Mahmood Amani
	Gholamreza Langari
Head of Department,	Stephen Holditch

August 2009

Major Subject: Petroleum Engineering

ABSTRACT

Development of a Well Intervention Toolkit to Analyze Initial Wellbore Conditions and Evaluate Injection Pressures, Flow Path, Well Kill, and Plugging Procedures.

(August 2009)

Amir Saman Paknejad, B.S., Petroleum University of Technology, Iran; M.S., Texas A&M University

Chair of Advisory Committee: Dr. Jerome Schubert

Every year, many wells are subject to well intervention operations for a variety of different reasons, such as Plug and Abandon (P&A) operations or well control situations. Wells that are not properly plugged, in addition becoming an inherent blowout threat, can act as a preferential pathway for surface contaminants to reach and impair ground water quality, and could cause injury to livestock, wildlife, or humans. Hence, federal code (or state code if in state waters) states that the wells must be plugged according to regulations.

If attempts with a surface intervention operation fail, a relief type subsurface intervention project is deemed appropriate. A relief well type of intersection into each target wellbore will create a hydraulic flow path suitable for plugging operations. The plugging operation will require the placement of permanent plugging fluids into the Target Well (TW) to meet Mineral Management Services (MMS), or other regulatory

agency, approved plugging criteria. Evidently, there is a need to design a method to insure that the scenarios are accurately defined, analyzed and the results can be effectively implemented to complete the plug and abandonment operations.

A software package, coupled with the skill of a hydraulic modeling specialist, could provide final resolution to and better understanding of the problem. However, considering uncertainties in some input information, there is a need to develop a multi-purpose package which enables the user to manipulate dynamically a wide range of input data in order to obtain the best fit. Therefore, the decision was made to develop a software package specifically built and designed to address the common problems encountered during well intervention projects.

The well intervention toolkit will be used to investigate the plugging and abandonment scenarios. The well intervention toolkit not only provides the critical input parameters to other commercial software but would also be a means to analyze and simulate the well intervention hydraulics.

DEDICATION

To my parents, Farkhondeh Kabirinejad and Kamal Paknejad, and my brother, Dr. Babak Paknejad.

To my fiancé, Dr. Parisa Ghodousi – Without your love and support none of this would have been possible.

ACKNOWLEDGEMENTS

I would like to thank my committee chair, Dr. Jerome Schubert, and my committee members, Dr. Hans Juvkam-Wold, Dr. Reza Langari, and Dr. Mahmood Amani for their guidance and support throughout the course of this research. Also, I would like to thank Dr. Peter Valko and Dr. Catalin Teodoriu.

I would like to thank Don Shackelford. This work would not have been possible without your help and guidance.

I would like to thank Boots and Coots Services, John Garner, Jim woodruff, Douglas Derr, and Jim Lagrone. Your support has been invaluable throughout the course of this project.

Thanks also go to my friends and colleagues and the department faculty and staff for making my time at Texas A&M University a great experience. I also want to extend my gratitude to friends and classmates Nima Zonoozi, Arash Haghshenas, Babak Akbarnejad, and Danial Kaviani.

Finally, thanks to my parents and brother for their encouragement and to my fiancé for her patience and love.

NOMENCLATURE

AOF	Absolute Open Flow
BHP	Bottom Hole Pressure
B_g	Gas formation volume factor
B_o	Oil formation volume factor
C_p	Specific heat at constant pressure, lbf-ft/lbm-^oR
C_t	Total system compressibility, psi^{-1}
C_v	Specific heat at constant temperature, lbf-ft/lbm-^oR
C_D	Choke discharge coefficient
d	Pipe diameter, m
d_{ch}	Choke diameter, inch
d_i	Inner diameter
dp_i	Pipe inner diameter
dp_o	Pipe outer diameter
dc_i	Casing inner diameter
Dq_g	Non-Darcy flow coefficient
FTP	Flowing Tubing Presure
g	Acceleration due to gravity, m/ s^2
GOR	Gas-Oil Ratio
h	Payzone thickness, ft
h_o	Height of the column of the oil, ft

h_{pf}	Height of the column of the plugging fluid, ft
IPR	Inflow Performance Relationship
IW	Intervention Well
k	Permeability, md
K	Specific heat ratio
KOP	Kick-Off Point
L	Length
MD	Measured Depth
MMS	Mineral Management Services
MW	Molecular Weight
p_c	Surface pressure rise, psi
p_{wf}	Wellbore flowing pressure, psi
P	Pressure at any point, psia
P&A	Plug and Abandon
PVT	Pressure-Volume-Temperature
P_{outlet}	Pressure at choke outlet, psi
P_b	Bubble point pressure, psi
P_{dn}	Downstream pressure at choke, psi
P_{up}	Upstream pressure at choke, psi
q	Flow rate, bbl/day
q_e	Fluid loss rate, ft^3/min
q_o	Oil production rate, STB/day

q_{sc}	Gas flow rate, Mscf/day
r_w	Well radius, ft
R	Ratio of the annulus inner and outer diameters
RN_B	Bubble Reynolds number
R_b	Bubble radius, m
R_s	Solution gas-oil ratio, scf/stb
S	Skin factor
SG	Specific Gravity
t	Transient time, hour
T	Temperature at any point, ^oR
TAMU	Texas A&M University
TFA	Total Flow Area
TVD	True Vertical Depth
TW	Target Well
v_b	Bubble velocity, m/sec
$\overline{v_g}$	Mean gas velocity
v_H	Homogeneous velocity
v_s	Gas-bubble slip velocity
V_{gas}	Gas volume in standard condition, scf
X_g	Influx volume, ft^3
X_m	Mud volume, ft^3
V_{oil}	Oil volume in stock tank condition, stb

X_w	Wellbore volume, ft^3
WC	Water Cut
X_g	Influx compressibility, psi^{-1}
X_m	Mud compressibility, psi^{-1}
X_w	Wellbore compliance, psi^{-1}
z	Gas compressibility factor
Z	Vertical change in elevation
α	Inclination angle
ϕ	Porosity, fraction
γ_g	Specific gravity of gas, dimensionless
γ_o	Specific gravity of oil, dimensionless
μ	Viscosity
μ_g	Gas viscosity, cp
μ_o	Oil viscosity, cp
μ_L	Liquid viscosity, Pas
ρ	Density
ρ_g	Density of the gas, ppg
ρ_o	Density of the oil, ppg
ρ_{pf}	Density of the plugging fluid, ppg
ρ_G	Gas density, kg/m^3
ρ_L	Liquid density, kg/m^3

TABLE OF CONTENTS

Page

ABSTRACT iii

DEDICATION v

ACKNOWLEDGEMENTS vi

NOMENCLATURE vii

TABLE OF CONTENTS xi

LIST OF FIGURES xiv

LIST OF TABLES xvi

1. INTRODUCTION 1

    1.1 Need for a New Software 6
    1.2 Development of the Well Intervention Toolkit 10
    1.3 Features and Advantages 10
    1.4 Toolkit Outputs 11

2. MODULE I: INFLOW PERFORMANCE RELATIONSHIPS (IPR) 13

    2.1 Single Phase IPR 14
        2.1.1 Transient Flow 15
        2.1.2 Pseudo Steady-State Flow 18
        2.1.3 Steady-State Flow 20
    2.2 Two Phase IPR 22
    2.3 Properties of Reservoir Fluids 23
        2.3.1 Gas Properties 23
            2.3.1.1 Specific Gravity 24
            2.3.1.2 Pseudo-Critical Pressure and Temperature ... 24
            2.3.1.3 Viscosity 25
            2.3.1.4 Compressibility Factor 28
            2.3.1.5 Density 28
            2.3.1.6 Formation Volume Factor 29
        2.3.2 Oil Properties 29
            2.3.2.1 Solution Gas-Oil Ratio, Rs 30

Page

2.3.2.2 Formation Volume Factor 31
2.3.2.3 Density 31
2.3.2.4 Viscosity 32
2.3.3 PVT Models 33
2.4 Computer Modeling 34
2.4.1 Reservoir Properties 34
2.4.2 PVT Analysis 35
2.4.3 Empirical IPR Data 36
2.4.4 Single Phase (Saturated) Oil Reservoir 38
2.4.5 Two Phase (Undersaturated) Oil Reservoir 38
2.4.6 Partial Two Phase Oil Reservoir 40
2.4.7 Single Phase Gas Reservoir 43
2.4.8 Nodal Analysis 44

3. MODULE II: SHUT-IN ANALYSIS 46

3.1 Flowing Wellbore 46
3.1.1 Theory 47
3.1.2 Application 51
3.2 Short Term Shut-In 53
3.2.1 Theory 54
3.2.1.1 Bubble Rise Velocity 57
3.2.2 Application 65
3.3 Intermediate Term Shut-In 68
3.3.1 Theory 68
3.3.2 Application 70
3.4 Long Term Shut-In 72
3.4.1 Theory 72
3.4.2 Application 73

4. MODULE III: PLUGGING SCENARIOS 75

4.1 Surface Piping 78
4.2 Intervention Well (IW) 79
4.3 Perforations 80
4.4 Target Well (TW) 81
4.4.1 Open System 82
4.4.1.1 Upward flow 84
4.4.1.2 Downward flow 87
4.4.1.3 Upward + Downward flow 89
4.4.2 Close System 90

Page

5. SUMMARY AND CONCLUSIONS 94

5.1 Further Work 95

REFERENCES 97

APPENDIX A 100

APPENDIX B 115

APPENDIX C 116

VITA 120

LIST OF FIGURES

		Page
Figure 1.1	Schematic of an Intervention Operation	2
Figure 1.2	Intersection Point vs. Completion	3
Figure 1.3	Flow Directions vs. Intersection Point	5
Figure 1.4	Basic Interception Scenario	7
Figure 2.1	Inflow vs. Outflow	14
Figure 2.2	Transient Flow	16
Figure 2.3	Pseudo-Steady State Flow	19
Figure 2.4	Steady State Flow	21
Figure 2.5	The Reservoir Properties Tab	35
Figure 2.6	PVT Analysis at 3328 psi and 153 ^{o}F	36
Figure 2.7	Empirical IPR Data for a Two Phase Flow	37
Figure 2.8	IPR Plot for a Single Phase Oil Reservoir	39
Figure 2.9	IPR Plot for a Two Phase Oil Reservoir	40
Figure 2.10	Partial Two Phase IPR Plot when Skin = 0	41
Figure 2.11	Partial Two Phase IPR Plot when Skin = 20	42
Figure 2.12	IPR Plot for a Single Phase Gas Reservoir	44
Figure 2.13	Nodal Analysis for a Flowing Wellbore	45
Figure 3.1	Dynamic Flow Analysis	48

Page

Figure 3.2 Distribution of Each Phase while Flowing 49

Figure 3.3 Pressure Profile for November 2001 Data 52

Figure 3.4 Pressure Profile for September 2004 Data 53

Figure 3.5 Hydrostatic Pressure Profile in Gas Column 56

Figure 3.6 Formation of the Gas Cap During the Shut-in Period 64

Figure 3.7 Short Term Shut-In 67

Figure 3.8 Fluid Exchange Point at the Payzone 69

Figure 3.9 Intermediate Term Shut-In Analysis 71

Figure 3.10 Long Term Shut-In Analysis 74

Figure 4.1 Flow Direction and Flow Type vs. Completion 76

Figure 4.2 The Plugging Scenarios 77

Figure 4.3 The Perforation Tunnel 81

Figure 4.4 Pressure vs. Pumped Volume Plot for Upward Flow through Tubing, Annulus, and Tubing + Annulus and Choke Sizes of 0.5, 0.75, and 1.5 inch 86

Figure 4.5 Pressure vs. Pumped Volume Plot for Downward Flow with Permeability Values of 100, 250, 500, and 1000 md 88

Figure 4.6 Pressure vs. Pumped Volume Plot for Combination Flow 90

Figure 4.7 Pressure vs. Pumped Volume Plot for Upward Flow through Tubing, Annulus, and Tubing + Annulus and Gas Percent Volumes of 25%, 50%, and 75% inch 93

LIST OF TABLES

Page

Table 2.1 Pressure-Rate Data 37

Table 3.1 Sample Static Pressure Survey 66

Table A1 Coefficients for Bubble Point Pressure in Vasquez and Beggs Correlation 109

Table A2 Coefficients for Oil Formation Volume Factor in Vasquez and Beggs Correlation 110

Table A3 Coefficients for Oil Compressibility in Vasquez and Beggs Correlation 110

Table A4 Coefficients for Oil Solution Gas in Velarde et al. Correlation 112

1. INTRODUCTION

Well intervention is defined as any operation carried out on an oil or gas well during, or at the end of its productive life, that alters the state of the well to provide well diagnostics or manage the production of the well. Every year many wells are subject to well intervention operations for variety of different reasons. Two of the reasons that interest us the most, are Plug and Abandon (P&A) operations and well control operations.

P&A is defined as preparing a wellbore to be shut-in and permanently isolated. Usually, after either logs determine there is insufficient hydrocarbon potential to complete the well, or after production operations have drained the reservoir the well is be closed permanently. Also, some well control issues may lead to P&A. Wells that are not properly plugged, in addition to be an inherent blowout threat, can act as a preferential pathway for surface contamination or to reach and impair ground water quality, and could cause injury to livestock, wildlife, environment, or humans.

Federal and state Codes state that the wells must be plugged according to regulations. If attempts with a surface intervention operation fail, a relief type subsurface intervention project is deemed as appropriate.

This dissertation follows the style of *SPE Drilling & Completion.*

A relief well type of intersection into each target wellbore will create a hydraulic flow path suitable for plugging operations designed to provide final resolution to the problem. The intervention well, as it is shown in **Fig. 1.1**, will have a shallow Kick Off Point (KOP). After the kick off, ranging methods are required to find and cross by or bypass the target well. Then, the intervention well will be drilled parallel to the target well down to the intersection point.

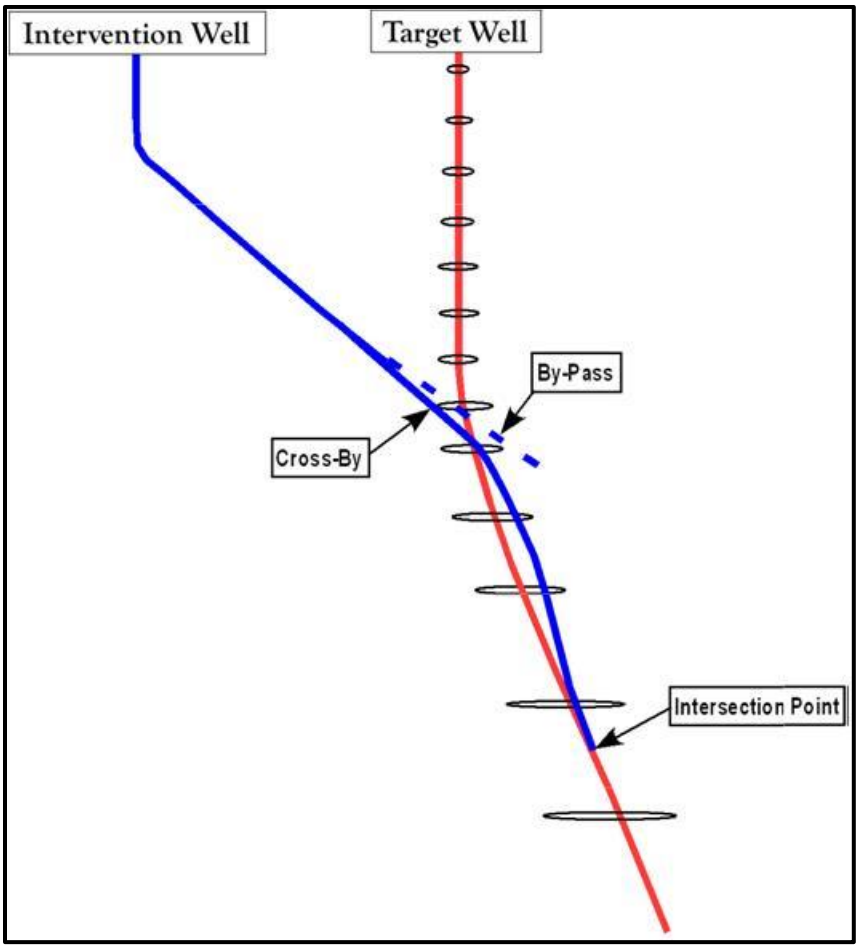

Figure 1.1 –Schematic of an Intervention Operation. Ranging methods are used to find and cross by or bypass the target well. Then, the intervention well will be drilled parallel to the target well down to the intersection point.

The intersection point will be determined according to the developed interception plan. **Fig. 1.2** shows that depending on the completion type, the intersection can be achieved in several points.

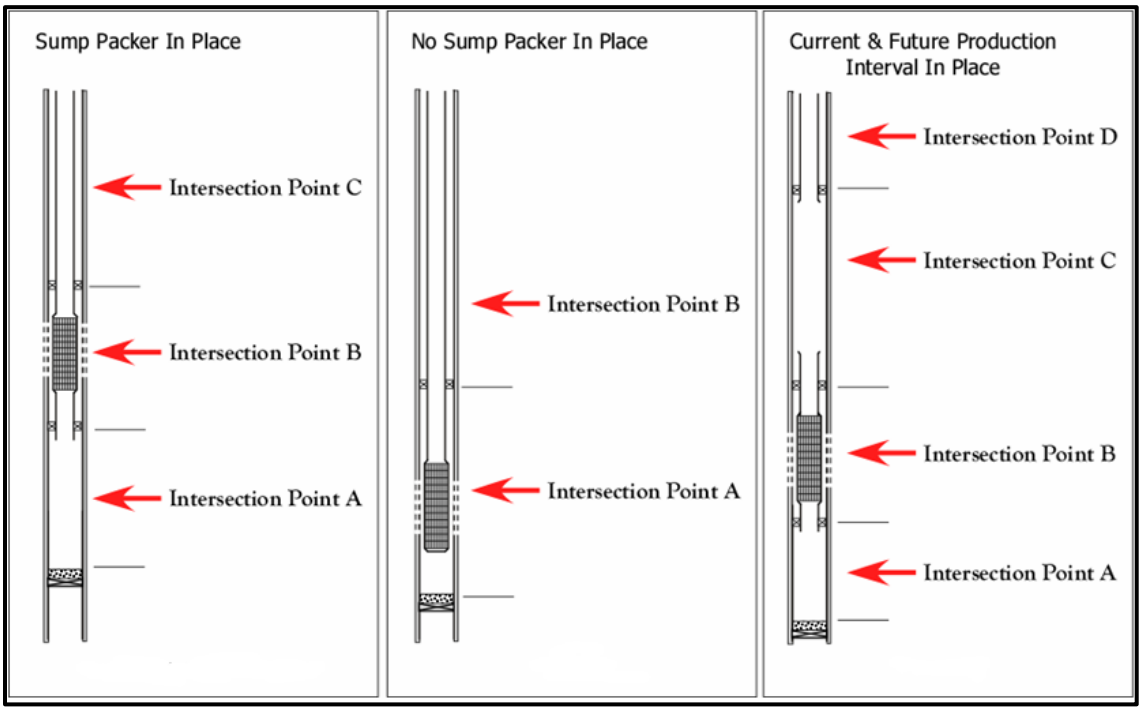

Figure 1.2 – Intersection Point vs. Completion. Depending on the completion type and intervention plan, the location of the intersection point may vary.

After achieving a suitable intersection, establishing hydraulic communication by a method which provides a functional and sustainable flow path is critical to the project's success. Typically, there are three methods to establish communication with the target well. These methods include, perforating, milling, and hydro-jetting. In a cased-hole environment, tubing conveyed perforating is the preferred method. After establishing

hydraulic communication with the Target Well (TW), two distinct hydraulic based operations will commence. The initial operation will include a stabilization period to equalize the hydrostatic differences of the fluids in the two wells thereby stopping any flow from a producing formation, followed by the plugging operation.

During the plugging operation, a minimum designed volume of cement should be pumped, under controlled conditions and within a set of approved operating parameters that will insure the cement is placed in a defined conduit which will permanently plug the well and prevent a future uncontrolled flow of reservoir fluids from the wellbore. However, it is important to adequately determine the communication path, pressure drop between the two wells, fluids to be pumped, required pumping rates, and maximum allowable surface pumping pressure. Based on the intersection point and completion type of the TW, as it shown in **Fig. 1.3**, the pumped plugging material may flow upward, downward, or in both directions.

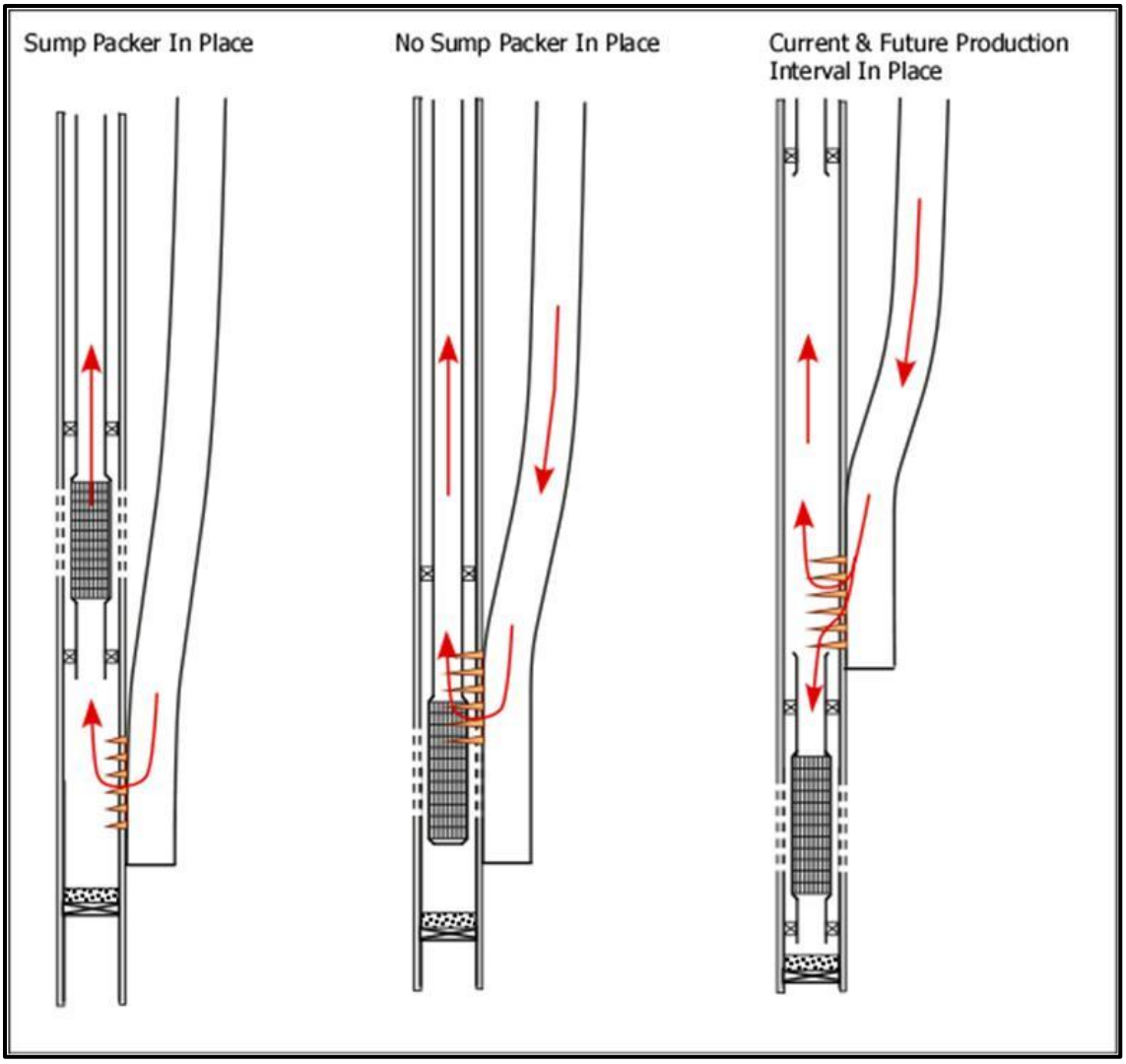

Figure 1.3 – Flow Direction vs. Intersection Point. Based on the intersection point, completion type, and intervention plan the pumped plugging material may flow upward, downward, or in both directions.

1.1 Need for a New Software

In order to continue with the intervention well planning and investigation, there is a requirement for information concerning reservoir conditions, well fluid components, and pressure profiles for the target wells. This information will be critical to achieve success during the drilling, hydraulic communication and plugging components of the intervention operations.

A basic interception scenario is displayed in **Fig. 1.4**. The fluid content inside the production tubing is unknown and must be defined for the hydraulic modeling and plugging operations. Heights, densities, fluid description and properties of the various fluids (produced water, oil and gas) are required. Also, the current and predicted reservoir conditions (static and flowing pressures, permeability, IPR curve(s), production fluid compositions, etc.) will be essential to produce an accurate analysis. Information based on a time variable is required to define the conditions at the time of the intersections.

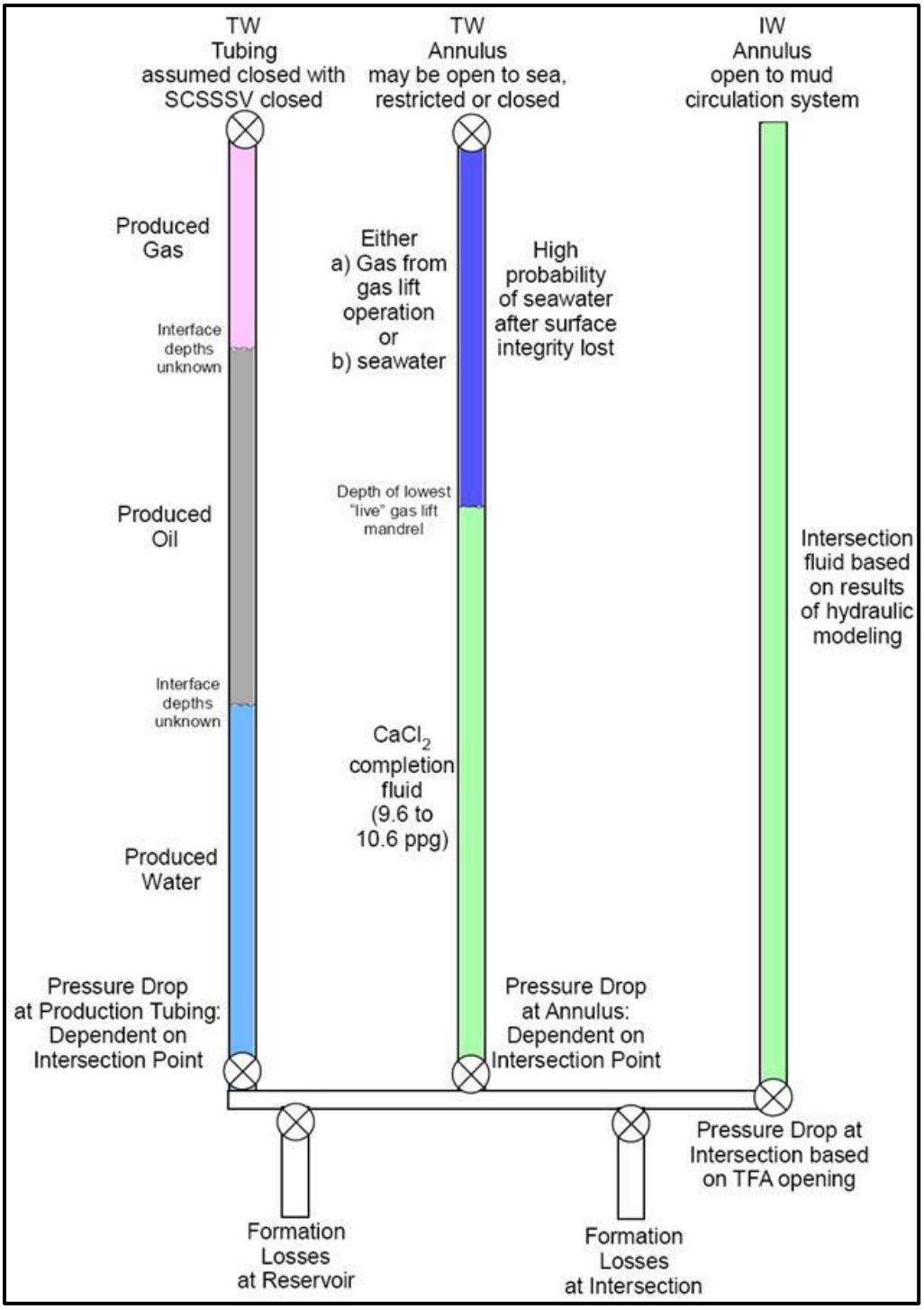

Figure 1.4 – Basic Interception Scenario. The pressure drops, losses, type and properties of the fluids should be determined prior to plugging operation.

In 1980 a software, named OLGA 2000, capable of simulating slow transients in two phase hydrocarbon transport pipelines, was developed based on a full-scale flow loop. Later, the software was upgraded for variety of applications such as dynamic kill scenarios. Since then, OLGA has evolved to become the industry's leading multiphase simulator. Therefore, the OLGA multiphase flow hydraulic software model, which coherently is developed as a production flow analysis tool, was selected to be employed to insure the scenarios are accurately defined, analyzed and the results can be effectively implemented to complete the plug and abandonment operations.

However, according to the set of runs performed with the OLGA, it was realized that to perform the complete analysis including well flow, pumps, drilling mode, TVD vs. MD, and fluid flow, OLGA needs to be loaded with the Advanced Well Module (AWM) and Black Oil Module (BOM). These specific modules are not included in the package currently available to TAMU. Hence, to proceed with these analyses, at the minimum, Advanced Well Module, Water Module, and any other module that can deal with the survey data of a well trajectory must be licensed with the current version.

Also, even upon the availability of the OLGA's advanced modules, the major part of the calculations such as; volume of contained fluids, pressure distribution along the wellbore, shut-in conditions after certain period of time, pressure loss through the perforations, and path and direction of the flow inside the TW should be calculated prior to perform by any simulation with OLGA.

Moreover, considering some uncertainties in the specific requested information, there is a need to develop a multi-purpose package which enables the user to dynamically manipulate a wide range of input data in order to obtain the best match. Some of the requested information includes:

- ✓ Current reservoir pressure of each target well producing reservoir,
- ✓ Estimated reservoir pressure at future time of well intervention based on build-up prediction model,
- ✓ Definition of the producing reservoir geologic characteristics including permeability, porosity, etc.,
- ✓ Production fluids (Oil, Gas & Water) properties: Specific Gravity (SG), Viscosity, etc.,
- ✓ Final Production Data: IPR, GOR, water, etc.,
- ✓ Gas Analysis,
- ✓ Oil Analysis.

Therefore, the decision was made to develop a software package, specifically built and designed to address these issues. The proposed software package should not only provide the critical input parameters to other commercial software but would also be a means to compare and confirm the results.

1.2 Development of the Well Intervention Toolkit

It was determined that the well intervention toolkit should include the following modules:

- Module 1: Inflow performance and nodal analysis of the well reservoir,
- Module 2: Calculation of wellbore dynamics at time of shut-in,
    - 2.1. Short term: Gas cap development, oil and water column development,
    - 2.2. Intermediate term: Loss of water column due to gravity separation,
    - 2.3. Long term: Development of maximum gas cap due to solution gas transfer.
- Module 3: Dynamics of plugging,
    - 3.1. Up flow only in target well,
    - 3.2. Down flow only in target well,
    - 3.3. Combination flow up and down in target well.

1.3 Features and Advantages

Some of the main features and advantages of the well intervention toolkit include;

- Analyzing of the well and the reservoir together,
- Handle the uncertainties in reservoir properties,

- Transient, pseudo-steady state, and steady state reservoirs,
- Saturated oil, undersaturated oil, and gas reservoirs,
- Built-in black oil models,
- Fluid properties adjusted for pressure and temperature effects,
- Multiphase flow,
- State-of-the-art dynamic visualization,
- Directional and inclined wellbores,
- Complex wellbore geometry,
- Handling leaks, chokes, and restrictions to the flow.

1.4 Toolkit Outputs

The well intervention toolkit provides the following information:

- Inflow Performance Curves (IPR), reservoir properties such as permeability, porosity, and drainage area, and wellbore conditions such as skin, payzone thickness, and flowing wellbore pressure.
- Nodal analysis can be performed based on two scenarios; 1) base pressure node at the surface, 2) base pressure node at the bottom of the well.
- Fluid density requirements in the Intersection Well (IW) to insure well control is maintained after establishing hydraulic communication.
- Sensitivity analysis of various fluids, densities, intersection depths, and reservoir conditions.

- Detailed plugging operation characteristics at varying well conditions.
- Required minimum Total Flow Area (TFA) between the two wells at the intersection point.
- Sensitivity analysis of plugging materials, placement heights, reservoir conditions, etc.
- Recommendations for achieving a safe and successful intersection and plugging of target wells.
- Comments on the prediction of the TW fluid compositions in the production tubing and annulus.
- Development of the hydraulic intersection and plugging plan.

2. MODULE I: INFLOW PERFORMANCE RELATIONSHIP (IPR)

An analytical relation between production rate and the reservoir's driving force, i.e., pressure difference of initial or average reservoir pressure and flowing bottomhole pressure, is called the Inflow Performance Relationship (IPR). Some of the key parameters of an intervention operation such as reservoir pressure, flowing bottomhole pressure, permeability, skin, porosity, payzone thickness, and etc. can be determined based on the IPR analysis. When planning an intervention, the mentioned IPR parameters combined with nodal analysis would be used to predict the BHP, surface flowing pressure, and flowing ability of the target well. Also, in the case of blowout, IPR is used to estimate the required injection rate to dynamically kill the well. As depicted in **Fig. 2.1**, the intersection of the inflow (IPR) and outflow (nodal analysis) helps to determine the flowing condition and required rate to kill the well.

Since, proper evaluation of pressure-rate data is crucial to the success of well intervention operations, a state of the art IPR analysis module is developed for the well intervention toolkit. The IPR module, module I, is designed in a way to enable the user to handle the uncertainties in reservoir properties and/or PVT data. Some of the most well-known PVT correlations, listed in section 2.3.3, are built into the software. Those in conjunction with the actual pressure-rate data (if available) would be used to get the best

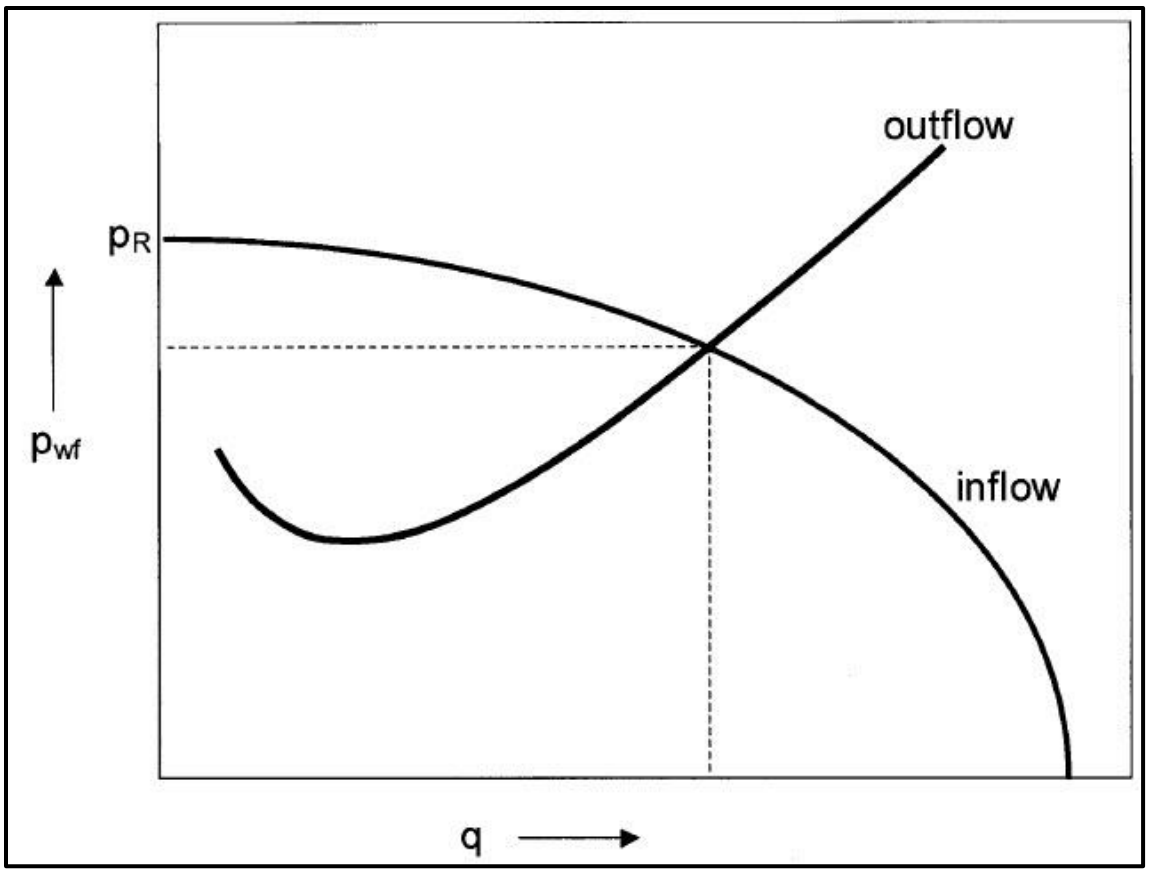

Figure 2.1 – Inflow vs. Outflow. The IPR and nodal analysis are used to investigate the flowing capability and determine the required kill rate.

match for the reservoir's properties such as pressure, permeability, skin, and pay zone thickness.

2.1 Single Phase IPR

The assumption of single-phase liquid flow is valid for under-saturated oil reservoirs or reservoir portions where the pressure is above the bubble point pressure. Since the

productivity index above the bubble point pressure is independent of production rate, the IPR curve for a single phase liquid reservoir is simply a straight line drawn from the reservoir pressure to the bubble point pressure. For gas reservoirs, the IPR curves are more complicated and the pressure dependency of gas properties such as compressibility and viscosity should be taken into account.

Depending on the conditions implied by the reservoir boundary, there are three distinct types of reservoir fluid inflow into the wellbore including transient flow, pseudo-steady-state flow, and steady-state flow. The IPR can be mathematically modeled on the basis of these inflow types.

2.1.1 Transient Flow

The transient flow occurs when the radius of pressure wave propagation from wellbore has not reached any boundaries of the reservoir (**Fig. 2.2**). During transient flow, because the developing pressure funnel is small relative to the reservoir size, the reservoir acts like an infinitively large reservoir.

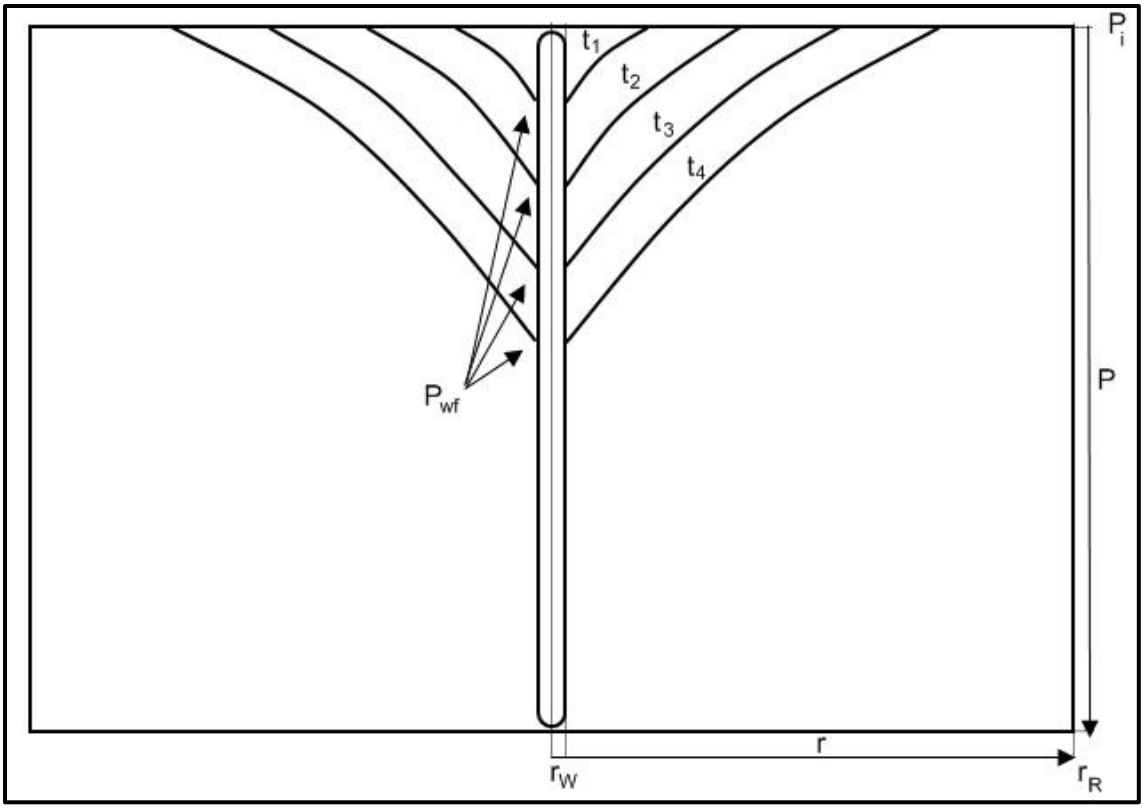

Figure 2.2 – Transient Flow. The pressure funnel has not reached to the reservoir boundaries.

In oil wells, because of constant wellhead pressure imposed by constant choke size, the wells are normally operated at constant bottomhole pressure. According to Guo et al. (2007), for a single phase oil flow in the reservoir, the transient flow into the wellbore is stated as;

$$q_o = \frac{kh\left(P_i - P_{wf}\right)}{162.6\, B_o\, \mu_o \left(\log t + \log \frac{k}{\varphi\, \mu_o\, c_t\, {r_w}^2} - 3.23 + 0.87S\right)}, \quad \text{..... (2.1)}$$

Where;

q_o = Oil production rate, STB/day

k = Permeability, md

h = Payzone thickness, ft

p_i = Reservoir initial pressure, psi

p_{wf} = Wellbore flowing pressure, psi

B_o = Oil formation volume factor

μ_o = Oil viscosity, cp

t = Transient time, hour

ϕ = porosity, fraction

C_t = Total system compressibility, psi^{-1}

r_w = Well radius, ft

S = Skin factor

Considering the fact that the radius of the pressure funnel, over which the pressure drawdown (p_i - p_{wf}) acts, increases with time, oil rate decreases with flow time. Therefore, the overall pressure gradient in the reservoir drops with time.

For gas wells, according to Economides et al. (1993), the transient solution is:

$$q_g = \frac{kh\left(m(P_i)-m(P_{wf})\right)}{1638\,T\left(\log t+\log\frac{k}{\varphi\,\mu_o\,c_t\,{r_w}^2}-3.23+0.87S\right)}, \quad \text{..... (2.2)}$$

Where;

$m(P) = \int_{P_b}^{P} \frac{2P}{\mu\, z}\, dP$, ... (2.3)

μ_g = Gas viscosity, cp

z = Gas compressibility factor

2.1.2 Pseudo-Steady-State Flow

Pseudo–steady-state flow occurs when the pressure at any point in the reservoir declines at the same constant rate over time (**Fig. 2.3**). During pseudo–steady-state flow, the pressure funnel has propagated to all no-flow boundaries such as; sealing faults, pinch-outs of pay zone, or boundaries of drainage areas of production wells.

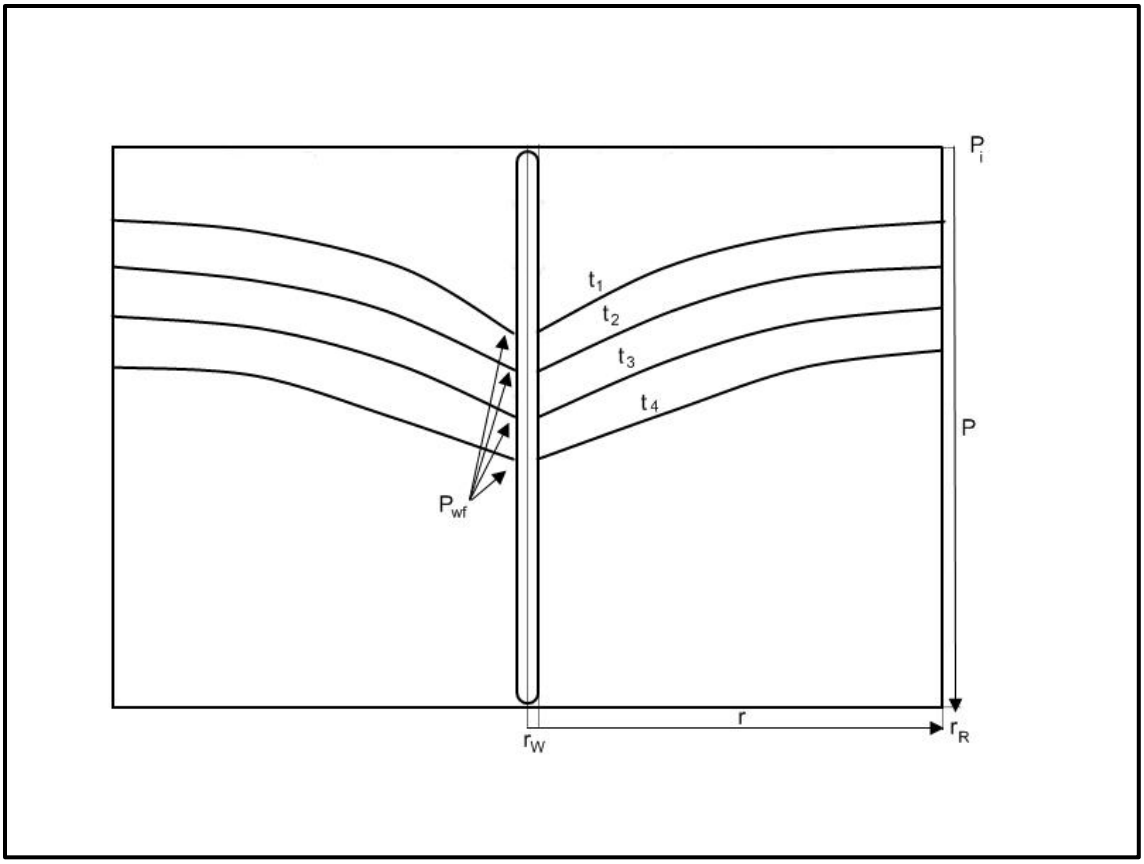

Figure 2.3 – Pseudo-Steady State Flow. The pressure funnel has propagated to the reservoir boundaries and the reservoir pressure declines at a constant rate.

Assuming single-phase oil flow, the pseudo–steady-state flow into the wellbore is stated as;

$$q_o = \frac{kh\left(\bar{P}-P_{wf}\right)}{141.2\ B_o\ \mu_o\left(\ln\frac{r_e}{r_w}-\frac{3}{4}+S\right)}, \quad \text{..... (2.4)}$$

The flow time required for the pressure funnel to reach the circular boundary can be expressed as;

$$t_{pss} = 1200 \frac{\varphi \, \mu_o \, c_t \, {r_e}^2}{k}, \quad \text{..... (2.5)}$$

For gas wells, the pseudo–steady-state flow is given by:

$$q_g = \frac{kh\left(m(\bar{P}) - m\left(P_{wf}\right)\right)}{1424 \, T\left(\ln\left(0.472 \frac{r_e}{r_w}\right) + S + Dq_g\right)}, \quad \text{..... (2.6)}$$

2.1.3 Steady-State Flow

Steady-state flow occurs when the pressure at any point in the reservoir remains constant over time (**Fig. 2.4**). During steady-state flow the pressure funnel has propagated to a constant pressure boundary such as an aquifer or a water injection well.

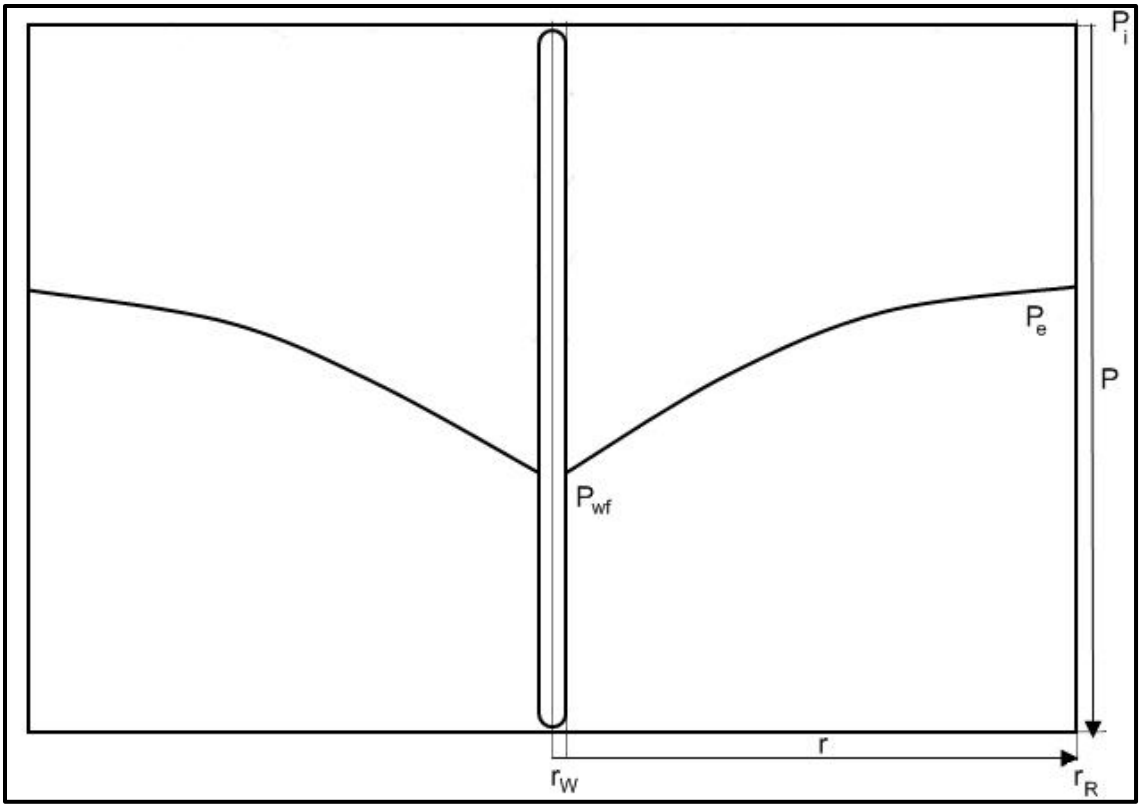

Figure 2.4 – Steady State Flow. The pressure funnel has propagated to a constant pressure boundary and the reservoir pressure stays constant over the time.

Assuming single phase oil flow, the steady-state flow into the wellbore is stated as;

$$q_o = \frac{kh\left(P_e - P_{wf}\right)}{141.2\ B_o\ \mu_o\left(\ln\frac{r_e}{r_w} + S\right)}, \quad \text{..... (2.7)}$$

For gas wells, the steady-state flow is given by:

$$q_g = \frac{kh\left(m(\bar{P}) - m\left(P_{wf}\right)\right)}{1424\ T\left(\ln\frac{r_e}{r_w} + S + Dq_g\right)}, \quad \text{..... (2.8)}$$

Where Dq_g is the non-Darcy flow coefficient.

2.2 Two Phase IPR

The linear IPR model mentioned earlier is valid for pressure values above the bubble point pressure. Below the bubble point pressure, as the solution gas escapes from the oil and become free gas, it occupies some portion of pore space, which reduces flow of oil. This effect is quantified by the reduced relative permeability. Also, oil viscosity increases as its solution gas content reduces. The combination of the relative permeability effect and the viscosity effect yields to lower oil production rate at a given bottomhole pressure. Therefore, the IPR curve deviates from the linear trend and the lower the pressure, the larger the deviation.

Only empirical equations are available for modeling IPR of two-phase reservoirs. Vogel's (1968) equation, still widely used in the industry, is written as;

$$q = q_{max}\left[1 - 0.2\left(\frac{P_{wf}}{P}\right) - 0.8\left(\frac{P_{wf}}{P}\right)^2\right], \quad \text{..... (2.9)}$$

Where $q_{\max}$ is an empirical constant and its value represents the maximum possible value of inflow into the wellbore or Absolute Open Flow (AOF). The $q_{\max}$ can be theoretically calculated based on reservoir pressure and productivity index above the bubble point pressure.

Generally, the bottomhole pressure, P_{wf}, is graphed versus the production rate, q.

2.3 Properties of Reservoir Fluids

Properties of oil and gas are fundamental for analyzing oil and gas inflow into the wellbore. Thus, using an appropriate Pressure-Volume-Temperature (PVT) model, the pressure based and temperature based properties of the fluids are to be determined. To comply with that, several PVT models, listed in section 2.3.3, are introduced into the IPR module. This section presents definitions of these fluid properties and some means of obtaining these property values other than experimental measurements**.**

2.3.1 Gas Properties

Gas properties are highly affected by the changes in pressure and temperature. Gas specific gravity and pseudo critical pressure and temperature depend on the composition of the gas. Viscosity, compressibility factor, density, and formation volume factor are more pressure dependent.

2.3.1.1 Specific Gravity

The specific gravity of a gas is defined as the ratio of the apparent molecular weight of the gas to that of air. The molecular weight of air is usually taken as equal to 28.97. Thus, the gas-specific gravity is given as;

$$\gamma_g = \frac{MW}{28.97}, \quad \text{..... (2.10)}$$

Where, *MW* is the apparent molecular weight of gas, which can be calculated on the basis of gas composition. Gas composition is usually determined in a laboratory and reported in mole fractions of components in the gas. Let y_i be the mole fraction of component *i*, using a mixing rule, the molecular weight is calculated as;

$$MW = \sum_{i=1}^{n} y_i \, MW_i , \quad \text{..... (2.11)}$$

Where, MW_i is the molecular weight of component *i*, and *n* is number of components. In general, gas specific gravity varies between 0.55 and 0.9.

2.3.1.2 Pseudo-Critical Pressure and Temperature

The critical properties of a gas can be calculated based on applying the mixing rule for critical properties of comprising compounds. However, when the gas composition is not

known, the specific gravity of the gas can be used to determine the pseudo critical value. Ahmed (1989) proposed correlations with impurity corrections for mixture pseudo-criticals as;

$$P_{pc} = 678 - 50(\gamma_g - 0.5) - 206.7\, y_{N_2} + 440\, y_{CO_2} + 606.7\, y_{H_2S}\,, \quad \text{..... (2.12)}$$

$$T_{pc} = 326 + 315.7(\gamma_g - 0.5) - 240\, y_{N_2} - 83.3\, y_{CO_2} + 133.3\, y_{H_2S}\,, \quad \text{..... (2.13)}$$

Applications of the pseudo-critical pressure and temperature are normally associated with pseudo-reduced pressure and temperature defined as;

$$P_{pr} = \frac{P}{P_{pc}}, \quad \text{..... (2.14)}$$

$$T_{pr} = \frac{T}{T_{pc}}, \quad \text{..... (2.15)}$$

where;

P = Pressure at any point, psia

T = Temperature at any point, ^{o}R

2.3.1.3 Viscosity

Generally, the specific gravity would be used to calculate the viscosity at atmospheric conditions. To adjust the atmospheric value with the downhole conditions, pseudo-

reduced pressure and temperature would be used to correct the atmospheric value. Carr et al. (1954) expressed the correlation of atmospheric viscosity in the form of;

$$\mu_l = \mu_{l_{HC}} + \mu_{l_{N_2}} + \mu_{l_{CO_2}} + \mu_{l_{H_2S}}, \quad \text{..... (2.16)}$$

Where;

$$\mu_{l_{HC}} = 8.188 \times 10^{-3} - 6.15 \times 10^{-3}\, Log(\gamma_g) +$$

$$(1.709 \times 10^{-5} - 2.062 \times 10^{-6}\, \gamma_g)T, \quad \text{..... (2.17)}$$

$$\mu_{l_{N_2}} = [9.59 \times 10^{-3} + 8.48 \times 10^{-3}\, Log(\gamma_g)]yN_2\,, \quad \text{..... (2.18)}$$

$$\mu_{l_{CO_2}} = [6.24 \times 10^{-3} + 9.08 \times 10^{-3}\, Log(\gamma_g)]yCO_2\,, \quad \text{..... (2.19)}$$

$$\mu_{l_{H_2S}} = [3.73 \times 10^{-3} + 8.49 \times 10^{-3}\, Log(\gamma_g)]yH_2S\,, \quad \text{..... (2.20)}$$

And based on the relation developed by Dempsey (1965);

$$\mu_r = ln\left(\frac{\mu_g}{\mu_l}\, T_{pr}\right) = a_0 + a_1 P_{pr} + a_2 {P_{pr}}^2 + a_3 {P_{pr}}^3 + T_{pr}\begin{pmatrix} a_4 + a_5 P_{pr} \\ + a_6 {P_{pr}}^2 + a_7 {P_{pr}}^3 \end{pmatrix} +$$

$${T_{pr}}^2\begin{pmatrix} a_8 + a_9 P_{pr} \\ + a_{10} {P_{pr}}^2 + a_{11} {P_{pr}}^3 \end{pmatrix} + {T_{pr}}^3\begin{pmatrix} a_{12} + a_{13} P_{pr} \\ + a_{14} {P_{pr}}^2 + a_{15} {P_{pr}}^3 \end{pmatrix}, \quad \text{..... (2.21)}$$

Where;

$a_0 = -2.46211820$

$a_1 = 2.97054714$

$a_2 = -0.28626405$

$a_3 = 0.00805420$

$a_4 = 2.80860949$

$a_5 = -3.49803305$

$a_6 = 0.36037302$

$a_7 = -0.01044324$

$a_8 = -0.79338568$

$a_9 = 1.39643306$

$a_{10} = -0.14914493$

$a_{11} = 0.00441016$

$a_{12} = 0.08393872$

$a_{13} = -0.18640885$

$a_{14} = 0.02033679$

$a_{15} = -0.00060958$

Once the values of μ_l and μ_r are determined, the corrected viscosity for the pressure and temperature is determined as;

$\mu_g = \frac{\mu_l}{T_{pr}} e^{\mu_r}$, ... (2.22)

2.3.1.4 Compressibility Factor

Gas compressibility factor, also known as "z-factor", reflects how much the real gas deviates from the ideal gas at a given pressure and temperature. Brill and Beggs (1978) developed the following correlation to estimate the z-factor;

$$z = A + \frac{1-A}{e^{B}} + C P_{pr}^{D} \ , \quad \text{..... (2.23)}$$

Where;

$$A = 1.39\left(T_{pr} - 0.92\right)^{0.5} - 0.36\, T_{pr} - 0.1 \ , \quad \text{..... (2.24)}$$

$$B = \left(0.62 - 0.23\, T_{pr}\right) P_{pr} + \left(\frac{0.066}{T_{pr} - 0.86} - 0.037\right) P_{pr}{}^{2} + \frac{0.32\, P_{pr}{}^{6}}{10^{E}} \ , \quad \text{..... (2.25)}$$

$$C = 0.132 - 0.32\, log\left(T_{pr}\right) \ , \quad \text{..... (2.26)}$$

$$D = 10^{F} \ , \quad \text{..... (2.27)}$$

$$E = 9\left(T_{pr} - 1\right) \ , \quad \text{..... (2.28)}$$

$$F = 0.3106 - 0.49\, T_{pr} + 0.1824\, T_{pr}{}^{2} \ , \quad \text{..... (2.29)}$$

2.3.1.5 Density

Applying the gas law for real gases and taking the compressibility into the account, the density in lb_m/ft^3 is calculated as;

$$\rho_g = \frac{2.7\,\gamma_g P}{z\,T}, \quad \text{..... (2.30)}$$

2.3.1.6 Formation Volume Factor

The ratio of gas volume at downhole condition to the gas volume at standard condition, the gas formation volume factor, is expresses as;

$$B_g = \frac{P_{sc}}{P} \times \frac{T}{T_{sc}} \times \frac{z}{z_{sc}} = 0.0283\,\frac{zT}{P}, \quad \text{..... (2.31)}$$

2.3.2 Oil Properties

Oil properties include solution gas–oil ratio (GOR), formation volume factor, compressibility, density, and viscosity. The bubble point pressure is the important variable in characterizing the oil. At pressures above the bubble point, oil (also called under-saturated oil) behaves like a liquid; below the bubble point, dissolved gas emerges out of the solution and becomes a free gas. The liquid phase of this multiphase solution is comprised of so-called “saturated” oil and water.

2.3.2.1 Solution Gas-Oil Ratio, R_s

The solution Gas-Oil Ratio (GOR) is defined as the amount of gas, at standard conditions, that will dissolve in unit volume of oil once both are taken to the reservoir pressure and temperature. The solution GOR, R_s, is defined as;

$$R_s = \frac{V_{gas}}{V_{oil}}, \quad (2.32)$$

Where;

R_s = solution gas-oil ratio, scf/stb

V_{gas} = gas volume in standard condition, scf

V_{oil} = Oil volume in stock tank condition, stb

At pressures above the bubble point, the solution GOR remains constant. Below the bubble point, the solution GOR varies with pressure and temperature; as pressure decreases, the solution GOR decreases. Solution GOR is often used as a base parameter for estimating other fluid properties when dealing with volumetric oil and gas calculations.

2.3.2.2 Formation volume factor

The ratio of volume of oil at reservoir's pressure and temperature to volume of oil in stock tank is defined as the formation volume factor. Its value is always greater than unity because oil dissolves more gas in reservoir condition than in stock tank condition; some of the solution gas would be liberated as pressure decreases. Above the bubble point, oil formation volume factor remains constant and it decreases as pressure decreases.

Formation volume factor is a base parameter for estimating other fluid properties associated with oil volumetric calculations.

2.3.2.3 Density

Density of oil, because of the gas content, varies with the pressure and the temperature. At standard condition, the density is evaluated by the API gravity. The relationship between the density of stock tank oil and API gravity is given as;

$$^{o}API = \frac{141.5}{\gamma_o} - 131.5\ , \quad \text{..... (2.33)}$$

Where;

γ_o = Specific gravity of stock tank oil, dimensionless

The density of oil, as a function of pressure and temperature, can be estimated on empirical correlations developed by several investigators. Ahmed (1989) suggested that the density of oil can be estimated as;

$$\rho_o = \frac{62.4\,\gamma_o + 0.0136\,R_s\,\gamma_g}{0.972 + 0.000147\left[R_s\sqrt{\frac{\gamma_g}{\gamma_o}} + 1.25\,T\right]^{1.175}}, \quad \text{..... (2.34)}$$

2.3.2.4 Viscosity

Viscosity, the resistance to flow of fluid, is a critical parameter in hydraulics calculations. Among the variety of developed empirical correlations, Standing's (1981) correlation for dead oil is expressed as;

$$\mu_{od} = \left(0.32 + \frac{1.8\times10^7}{o_{API}{}^{4.53}}\right)\left(\frac{360}{T+200}\right)^A, \quad \text{..... (2.35)}$$

Where;

$A = 10^{\left(0.43+\frac{8.33}{o_{API}}\right)}$

μ_{od} = Viscosity of dead oil, cp

And for saturated crude oil;

$$\mu_{ob} = 10^a\,\mu_{od}^b, \quad \text{..... (2.36)}$$

Where;

$a = R_s(2.2 \times 10^{-7} R_s - 7.4 \times 10^{-4})$

$b = \frac{0.68}{10^c} + \frac{0.25}{10^d} + \frac{0.062}{10^e}$

$c = 8.62 \times 10^{-5} R_s$

$d = 1.1 \times 10^{-3} R_s$

$e = 3.74 \times 10^{-3} R_s$

μ_{ob} = Viscosity of saturated crude oil, cp

Furthermore, the correlation for unsaturated crude oil is expressed as;

$\mu_o = \mu_{ob} + 0.001(P - P_b)\left(0.024\,\mu_{ob}^{1.6} + 0.38\,\mu_{ob}^{0.56}\right)$, ... (2.37)

Where;

P_b = Bubble point pressure, psia

2.3.3 PVT Models

In order to obtain the best estimates of the interrelated properties, several PVT models are included in the IPR module. With the specific gravities of oil and gas being the only inputs, properties of the crude oil could be calculated based on one of the following PVT models;

- Al-Marhoun Correlations (Saudi Arabian Oil)
- Glaso Correlations (North Sea Oil)
- Hanafy *et al*. Correlations (Egyptian Oil)
- Petrosky and Farshad Correlations (Gulf of Mexico Oil)
- Standing Correlations (California Oil)
- Vasquez and Beggs Correlations (Generally Applicable)
- Velarde *et al*. Correlations (Generally Applicable)

The models, listed above, are described in more details in appendix A.

2.4 Computer Modeling

The IPR module consists of six sub-modules, each represented by a tab in the toolkit's interface. The sub-modules, also shown in **Fig. 2.5**, are: reservoir properties, PVT analysis, empirical IPR data, single phase (saturated) oil reservoir, two phase (undersaturated) oil reservoir, partial two phase oil reservoir, and single phase gas reservoir.

2.4.1 Reservoir Properties

This sub-module is designed to input the basic reservoir properties. This is just an input screen and there are no calculations involved. The input values are used as the initial

values in order to for the models to begin running. The key input values could be changed later on through the "manipulation" options. Hence, in the case of high uncertainties in input values, one could enter approximate values. The key input reservoir properties include; pressure, permeability, payzone thickness, skin, and production time. The non-changeable reservoir properties include; temperature, reservoir radius, wellbore radius, porosity, and total compressibility of the system. The complete list of input parameters, according to the data provided in appendix B, is shown in **Fig. 2.5**.

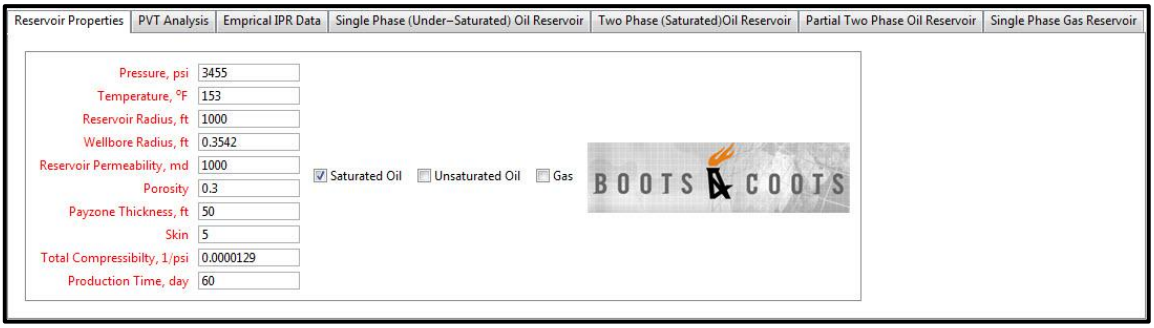

Figure 2.5 - The Reservoir Properties Tab.

2.4.2 PVT Analysis

Once the basic reservoir properties are entered, the oil and gas specific gravity and gas impurity mole fractions are required to calculate the fluid properties based on the chosen correlations presented in the "PVT Analysis" tab. As it is shown in **Fig. 2.6**, based on the selected PVT model, the gas and oil properties are automatically calculated. It should be

noted that, the value of each property could be either calculated based on the selected PVT model, or could be defined by the user. If a value is defined by the user, all other related properties would be calculated based on the user defined value. Note that, based on another study, similar data are provided in appendix A for comparison purposes.

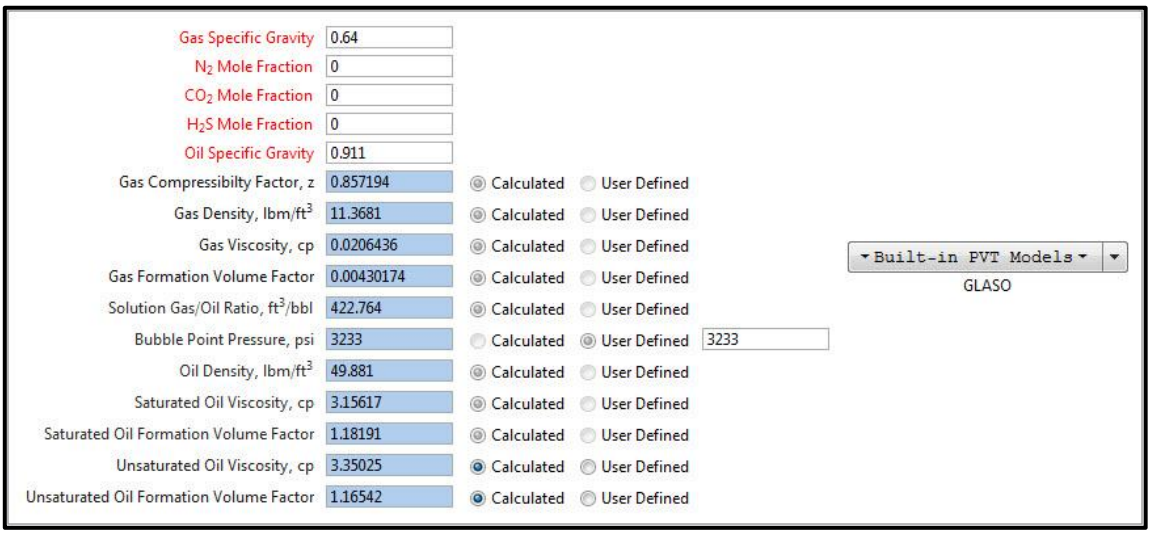

Figure 2.6 - PVT Analysis at 3328 psi and 153 ^{o}F.

2.4.3 Empirical IPR Data

When pressure versus rate data is available for a well, such data could be plotted along with the IPR curve. This is a key feature that enables the user to manipulate the values of reservoir properties to fit the IPR curve with the empirical data. Once the match is found, the adjusted values would substitute the initial values entered in the "reservoir properties" tab. In the case of two phase flow, the total rate could be calculated based on

the gas, oil, and water rates. Using the data provided in Table 2.1, two sample pressure-rate data points for a two phase flow are shown in **Fig. 2.7**.

Table 2.1 – Pressure-Rate Data

Date	FTP, psi	BHP, psi	BOPD	MSCF/D	BWPD	Production
11-01	550	3155	421	160	515	Flowing
09-04	250	3032	216	73	1137	Gas Lift

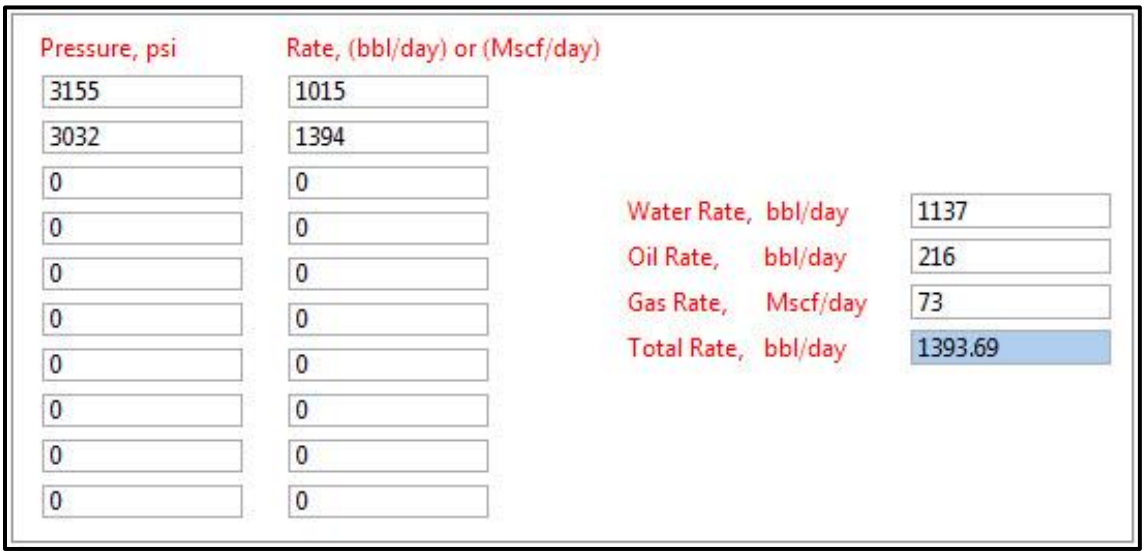

Figure 2.7 – Empirical IPR Data for a Two Phase Flow. The water, oil, and gas rates are converted into a single liquid rate to be used in the IPR plots.

2.4.4 Single Phase (Saturated) Oil Reservoir

The single phase oil IPR correlations mentioned earlier are employed to generate the transient, pseudo-steady-state, and steady-state IPR curves. **Eqs. 2.1**, **2.4**, and **2.7** are used to calculate the production rate over a range of flowing bottomhole pressure. For a single phase oil IPR plot, the bottomhole flowing pressure could vary anywhere from the reservoir pressure to the bubble point pressure. Using the IPR plot, at any flowing bottomhole pressure, the associated rate can be predicted. With the bubble point pressure of 2500 psi, the linear trend in IPR plot is shown in **Fig. 2.8**. The blue, brown, and red lines represent transient flow, pseudo-steady state flow, and steady state flow, respectively.

2.4.5 Two Phase (Undersaturated) Oil Reservoir

The two phase IPR correlation mentioned earlier (**Eq. 2.9**) is employed to generate the transient, pseudo-steady-state, and steady-state IPR curves. Also, the two phase pressure-rate data, red points in the lower right part of the **Fig. 2.9**, are incorporated into the IPR Plot. According to the pressure-rate data, given in **Table 2.1**, after 60 days the well is still producing in transient state. However, 3 years later, the well is producing in steady-state condition.

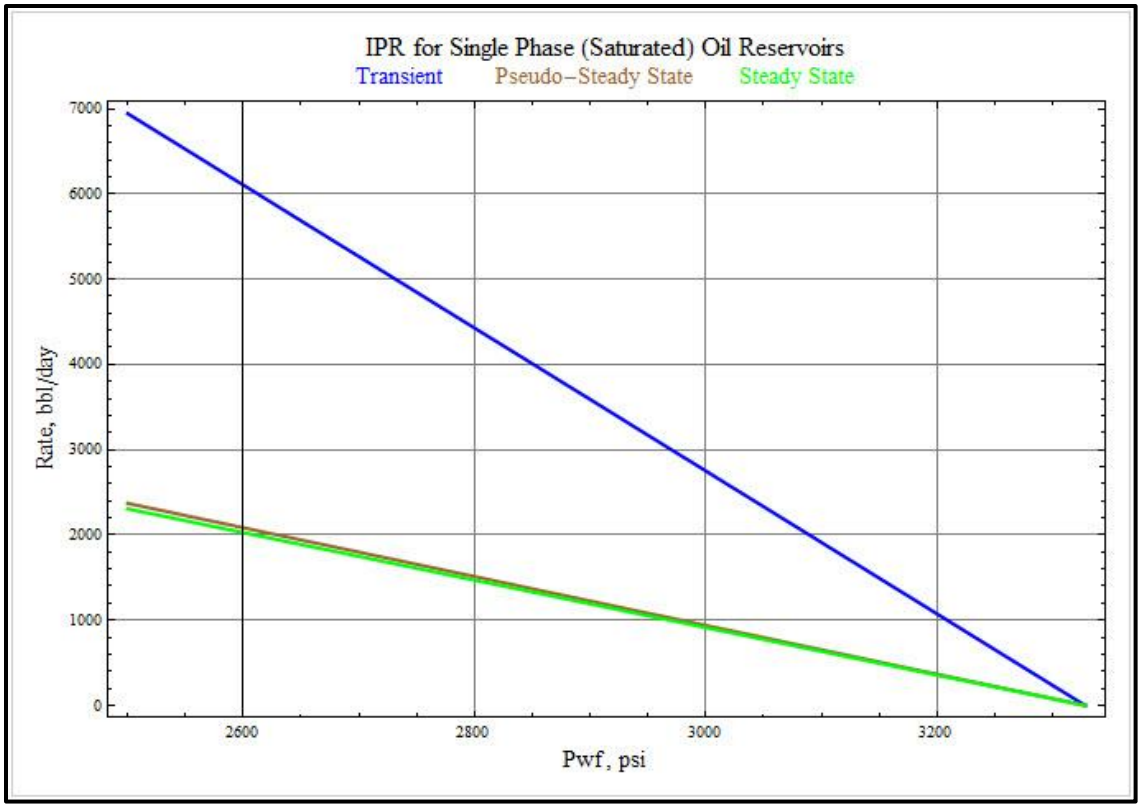

Figure 2.8 – IPR Plot for a Single Phase Oil Reservoir.

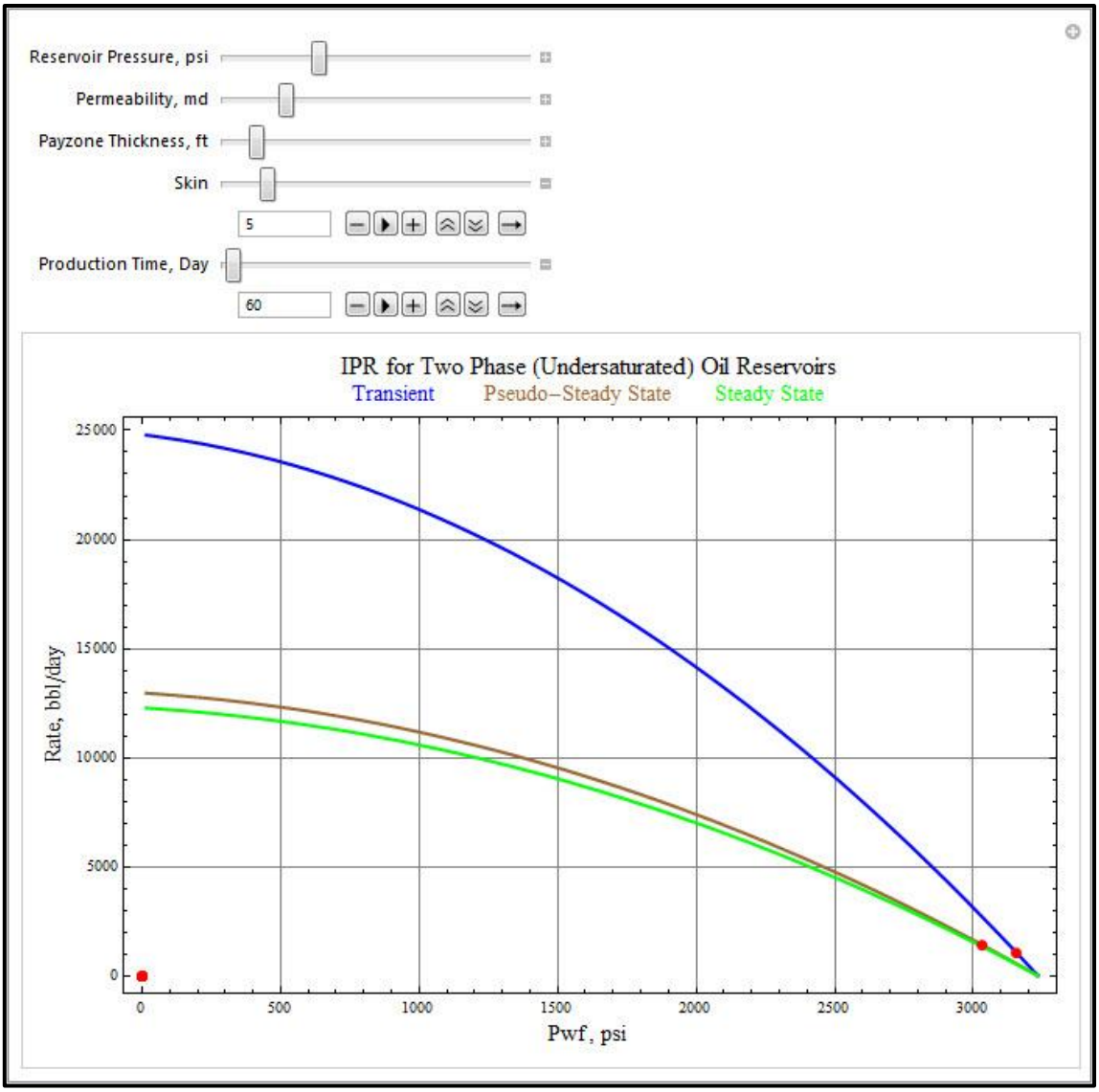

Figure 2.9 – IPR Plot for a Two Phase Oil Reservoir. Plotting the three different flow regimes enables the user to detect any change in the state of the flow.

2.4.6 Partial Two Phase Oil Reservoir

The partial two phase IPR is a combination of a single phase IPR for pressures above the bubble point and two phase IPR for pressures below the bubble point. That is, a straight

single phase portion followed by a two phase curve. Here is an example to show the use of manipulation in fitting the empirical data with the developed curves. Assuming a case with the skin of zero, as it is shown in **Fig. 2.10**, the predicted IPR curves and the empirical data (red points in the lower right part of the graph) do not match.

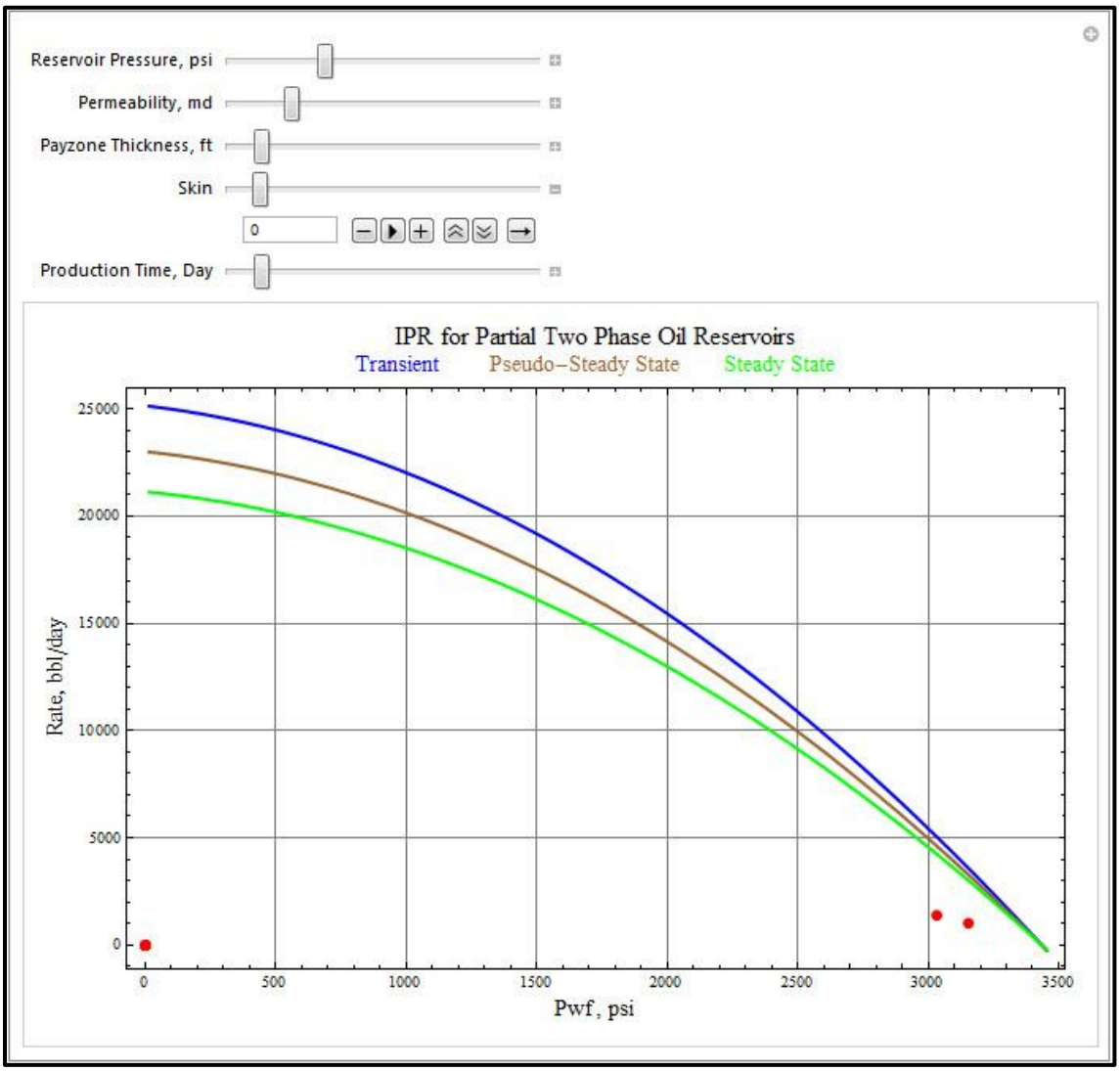

Figure 2.10 – Partial Two Phase IPR Plot when Skin = 0. The plot covers the flowing bottomhole pressures above and below the bubble point.

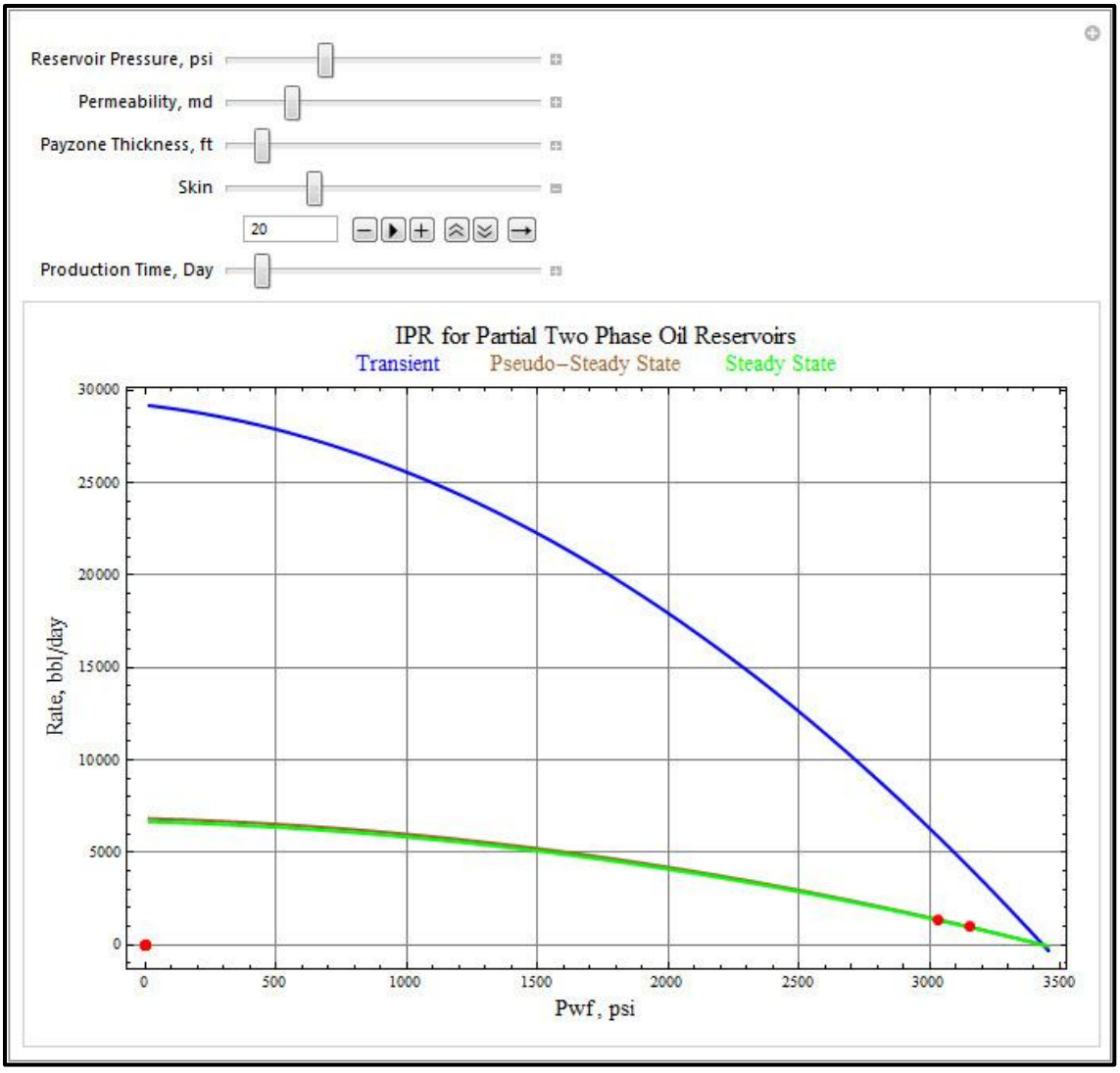

Figure 2.11 - Partial Two Phase IPR Plot when Skin = 20. Manipulation of the parameters enables the user to match the curves with the actual pressure-rate data.

Now, the same case, with the skin being increased to 20, the steady-state and pseudo-steady-state curves match with the data points (**Fig. 2.11**).

Thus, it could be concluded that the initial skin value of zero is not a valid assumption and the skin value should be replaced by the latest value. Note that, in most cases, there are several parameters that could be manipulated to obtain a match.

2.4.7 Single Phase Gas Reservoir

In spite of more complexity, similar to the saturated and undersaturated oil reservoirs, the IPR plot could be constructed for single phase gas reservoirs. Using the built-in functions for the gas compressibility, viscosity, and pseudo pressures, the IPR plot for a single phase gas is shown in **Fig. 2.12**.

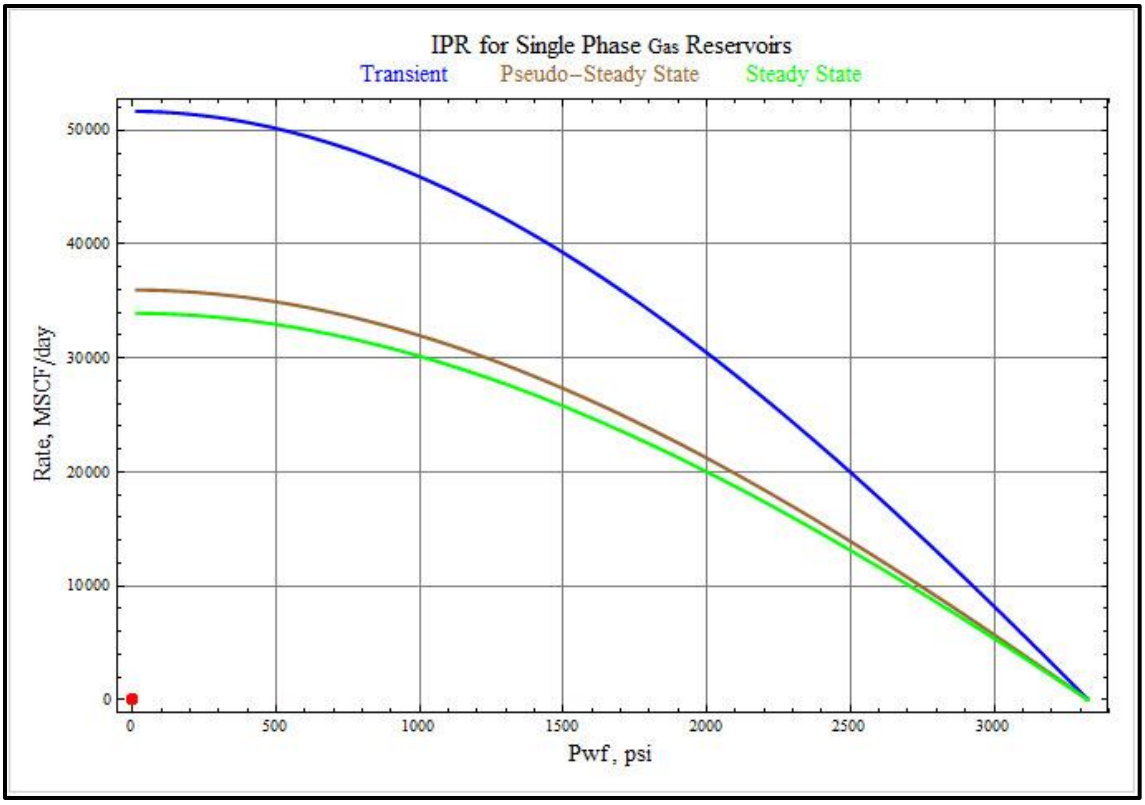

Figure 2.12 - IPR Plot for a Single Phase Gas Reservoir.

2.4.8 Nodal Analysis

A node is selected at the bottom of the flowing well. The bottomhole flowing pressure at this node can be calculated from two sets of equations upstream and downstream of the flow. The plot of inflow to the node, as explained earlier, would yield to the developed IPR curves. The outflow of the node is

$$P_{wf} = P_{exit} + P_{friction} + P_{hydrostatic} \ , \quad \text{..... (2.38)}$$

When **Eq. 2.38** is plotted as a function of flow rate (**Fig. 2.13)** along with the IPR curves, there exists an interception point. The pressure and rate at the interception point would indicate the conditions at which one could expect the well to flow.

The pressure at the top of the well, water cut, WC, and producing GOR are required parameters to perform the nodal analysis. The nodal analysis is a common way to predict whether a well will flow (and at what rate and pressure) under certain conditions.

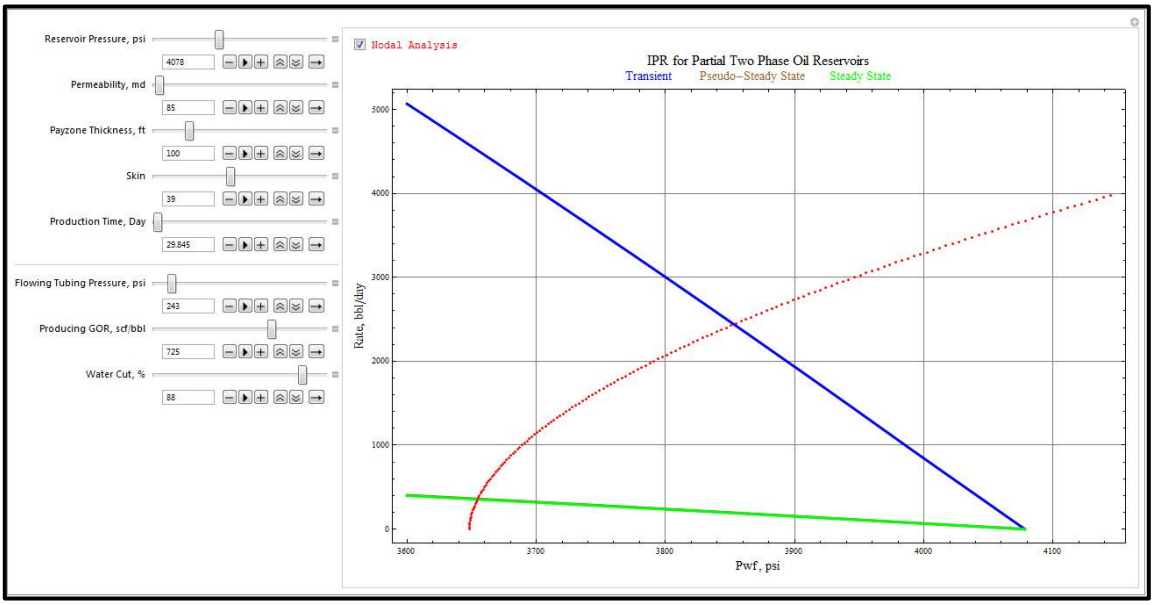

Figure 2.13 – Nodal Analysis for a Flowing Wellbore. Depending on the reservoir flowing conditions (transient flow or steady state flow) there are two points of intersection between the outflow curve (red) and the inflow curves.

3. MODULE II: SHUT-IN ANALYSIS

In well intervention operations, the target well could be either a flowing well or a well which has been shut-in for a certain period of time. In the case of flowing wells, analyzing the inflow rates, flowing bottomhole and surface pressures, and well fluid components is essential to a successful well intervention project. In shut-in wells, estimation of surface and bottomhole pressure profiles at the time of intervention and volumes (heights) of each produced fluid inside the well is required for further evaluations. In this section, the flowing wellbore analysis is presented first and then the shut-in analysis. Based on the duration of the shut-in period, the shut-in analysis is divided into three categories, including; short term (hours) shut-in, intermediate term (days) shut-in, and long term (years) shut-in.

3.1 Flowing Wellbore

Since, oil and gas properties are pressure and temperature dependent, these properties change with their location inside the producing well. Similar to the nodal analysis, in order to simulate the fluid flow inside the producing well, the wellbore is to be divided into discrete sections (e.g. 100 ft intervals). Then, using the principle of pressure continuity at each section, fluid properties are evaluated locally. It should be noted that

there is only one unique pressure value at a given node regardless of whether the pressure is evaluated from the performance of upstream or downstream flow.

3.1.1 Theory

In general, the rates at the surface and the flowing pressure at the bottom are known. To calculate the flowing pressure at the surface, first, the surface rates are converted to the equivalent downhole rates. Then, beginning with the section at the point of inflow into the wellbore, the flow into and out of each section is analyzed, section by section, all the way up to the surface. In other words, according to **Fig. 3.1**, with a known pressure at the bottom of the first section, the calculated pressure at the top of that section would be the known pressure at the bottom of the next section. The fluids pressure and temperature related properties along with the liberation and expansion of the gas are taken into the account, based on the rate of flow into and out of a section, to calculate the frictional pressure loss and hydrostatic pressure.

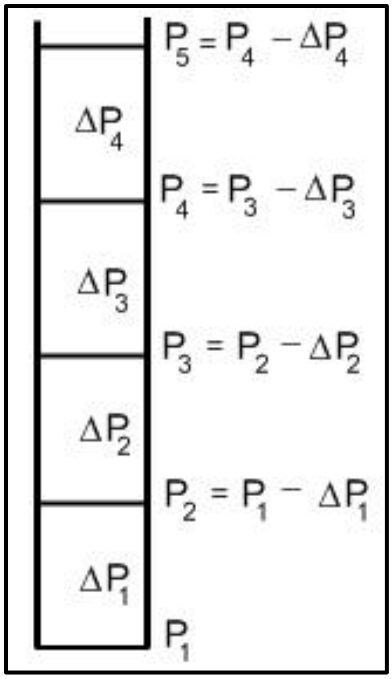

Figure 3.1 – Dynamic Flow Analysis. With a known pressure at the bottom of the first section, the calculated pressure at the top of that section would be the known pressure at the bottom of the next section.

Assuming multiphase (gas, oil, and water) flow into the wellbore, as it is shown in **Fig. 3.2**, in a controlled volume (section), the volume occupied by each fluid is proportional to the ratio of the fluid inflow rate to the total inflow rate.

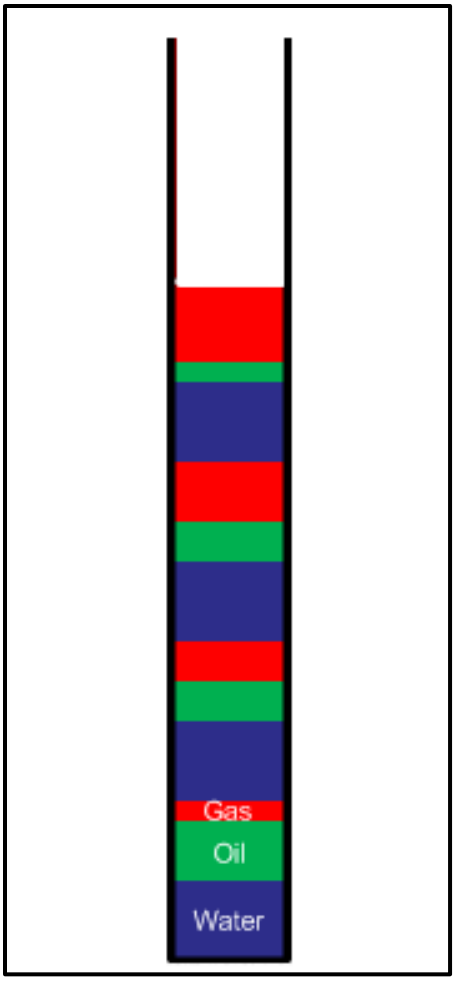

Figure 3.2 – Distribution of Each Phase while Flowing.

Applying the concept depicted in **Fig. 3.2**, the frictional pressure loss correlations (see appendix C) are used to calculate the pressure profile for the flowing wellbore. The general form of the governing equation at each section, with all pressure and temperature related properties calculated specifically for that section, can be presented as;

$$P_{top} = P_{bottom} -$$

$$[waterfraction_{P,T}(water\ frictional\ loss + water\ hydrostatic) +$$

$$oilfractionP,\ T\ oil\ frictional\ loss + oil\ hydrostatic + gasfractionP,\ T\ gas\ frictional\ loss + gas\ hydrostatic, \quad \text{..... (3.1)}$$

Where;

$$waterfraction_{P,T} = \frac{water\ rate}{\left(\begin{array}{c} water\ rate \\ + \\ oil\ rate \times oil\ formation\ volume\ factor \\ + \\ \left(\begin{array}{c} gasrate \times gas\ formation\ volume\ factor \\ - \\ oil\ rate \times solution\ gas\ ratio \times gas\ formation\ volume\ factor \end{array}\right) \end{array}\right)}, \quad \text{.. (3.2)}$$

$$oilfraction_{P,T} = \frac{oil\ rate}{\left(\begin{array}{c} water\ rate \\ + \\ oil\ rate \times oil\ formation\ volume\ factor \\ + \\ \left(\begin{array}{c} gasrate \times gas\ formation\ volume\ factor \\ - \\ oil\ rate \times solution\ gas\ ratio \times gas\ formation\ volume\ factor \end{array}\right) \end{array}\right)}, \quad \text{..... (3.3)}$$

$$gasfraction_{P,T} = \frac{\left(\begin{array}{c} gasrate \times gas\ formation\ volume\ factor \\ - \\ oil\ rate \times solution\ gas\ ratio \times gas\ formation\ volume\ factor \end{array}\right)}{\left(\begin{array}{c} water\ rate \\ + \\ oil\ rate \times oil\ formation\ volume\ factor \\ + \\ \left(\begin{array}{c} gasrate \times gas\ formation\ volume\ factor \\ - \\ oil\ rate \times solution\ gas\ ratio \times gas\ formation\ volume\ factor \end{array}\right) \end{array}\right)}, \quad \text{..... (3.4)}$$

Note that, for the pressures above the bubble point pressure, the gas rate and consequently the gas fraction would be zero since there is no free gas.

3.1.2 Application

Generally, the presence of any restriction in the path of reservoir fluid flow into the reservoir (i.e. skin) would make the flowing bottomhole pressure different than the reservoir pressure. Therefore, when no downhole pressure gauge in place, there is always a degree of uncertainty in flowing bottomhole pressure values. However, as surface pressure gauges are most often available, an agreement between the calculated and measured flowing surface pressure could yield a better estimate of the flowing bottomhole pressure.

For instance, using the recorded rates and flowing bottomhole pressure presented in **Table 2.1**, should yield the same flowing surface pressure. As it is shown in **Fig. 3.3**, for the first set of data (November 2001) the predicted surface pressure is in agreement with the measured (Flowing Tubing Pressure) FTP value shown in **Table 2.1**.

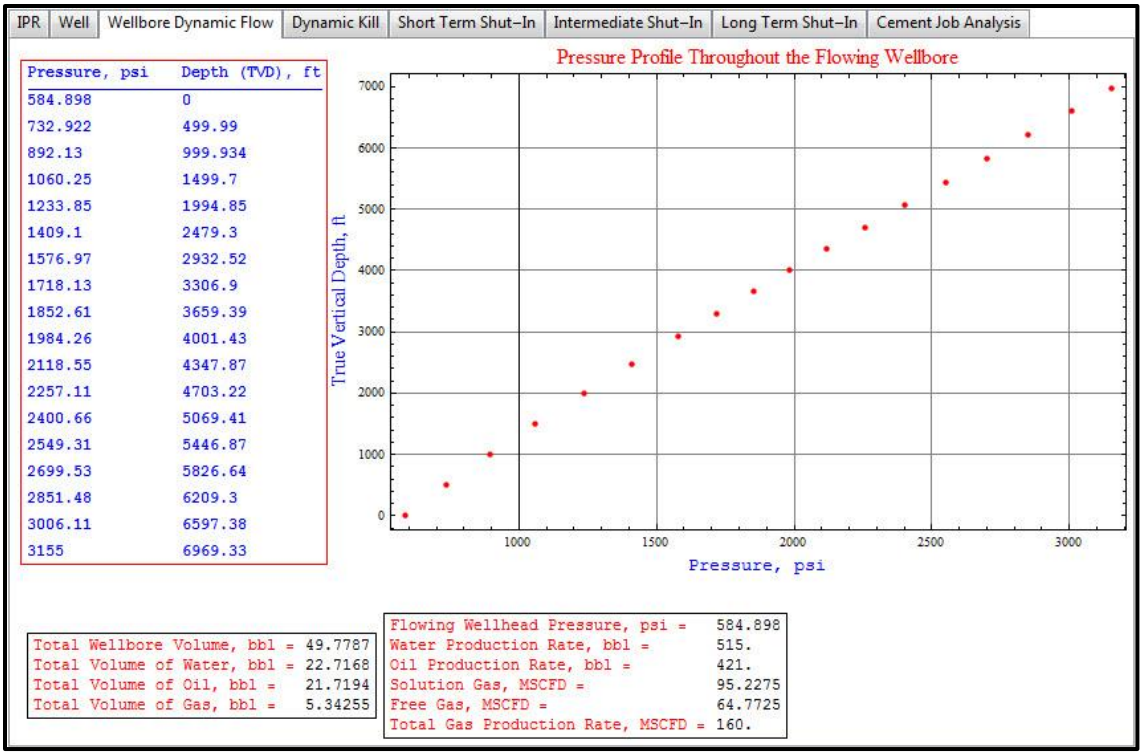

Figure 3.3 – Pressure Profile for November 2001 Data.

However, when using the second set of data (September 2004), the predicted surface pressure (**Fig. 3.4**) is different from the measured FTP value (**Table 2.1**). That is because, at the time, the well has been on gas-lift and some additional pressure has been exerted on the gauge at the surface. Otherwise, the flowing surface pressure would have been less than measured.

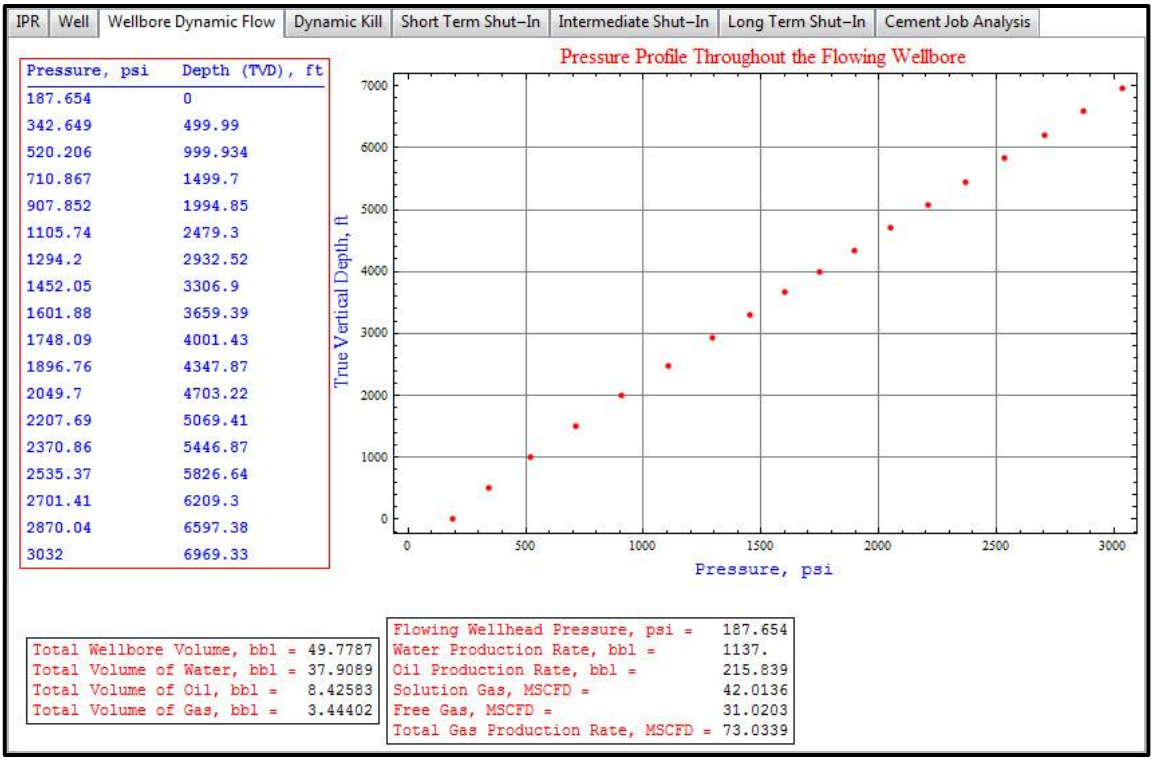

Figure 3.4 – Pressure Profile for September 2004 Data.

3.2 Short Term Shut-In

Once the well is shut-in, because of the difference in the densities of the contained fluids, the fluids begin to separate. As a result, the fluid with the highest density (water) accumulates in the bottom sections and the fluid with the lowest density (gas) migrates to the upper sections of the well. After a certain period of time, depending on the bubble rise velocity, the separation of the fluids would yield to the formation of gas cap, oil column, and water column.

3.2.1 Theory

To simulate the fluids separation, first, it is assumed that as gas pockets migrate to the top, with no expansion, the higher pressures of the lower sections are conveyed to the top of the wellbore as;

$$P_{@top} = \frac{P_{@bottom}\ T_{@top}\ Z_{@top}}{T_{@bottom}\ Z_{@bottom}}, \quad \text{..... (3.5)}$$

Then, as the gas pockets join the gas cap at the top, the gas pocket expands and the average pressure of the mixture is given by;

$$\frac{P_{pocket}\ V_{pocket}}{Z_{pocket}} + \frac{P_{gas\ cap}\ V_{gas\ cap}}{Z_{gas\ cap}} = \frac{P_{mix}\ V_{mix}}{Z_{mix}}, \quad \text{..... (3.6)}$$

However, since the mixture volume, V_{mix}, is not simply the sum of the gas pocket volume, V_{pocket}, and the existing gas cap volume, $V_{gas\ cap}$, the right hand side of the equation should be adjusted by imposing the following restriction;

$$P_{bottom\ hole} = P_{water\ column} + P_{oil\ column} + P_{gas\ cap}, \quad \text{..... (3.7)}$$

Where;

$$P_{gas\ cap} = \frac{P_{mix}\,V_{mix}}{Z_{mix}} \times \frac{Z_{mix\ adjusted}}{V_{mix\ adjusted}} + Hydrostatic\ Pressure\ of\ Lower\ Half\ of\ the\ Gas\ Column\ , \quad \text{..... (3.8)}$$

Note that, because $P_{gas\ cap}$ is calculated as the average gas pressure at the middle of gas column, only the hydrostatic pressure of the lower gas column needs to be considered. As it is shown in **Fig. 3.5**, in relationship with depth, the hydrostatic pressure of a column of gas is not linear. Hence, **Eq. 3.9** is used to estimate the hydrostatic pressure of the lower half.

$$P_{bottom} = e^{\frac{0.0375\ \gamma_g TVD}{2\ ZT}} P_{surface}\ , \quad \text{..... (3.9)}$$

Clearly, the components of **Eq. 3.8** are interrelated and as the volume of the gas (height of the gas column) changes, the heights of the oil and water columns and consequently their corresponding hydrostatic pressures change too. Also, bearing in mind that the gas compressibility factor is a function of pressure, several iterations are needed to proceed with each step.

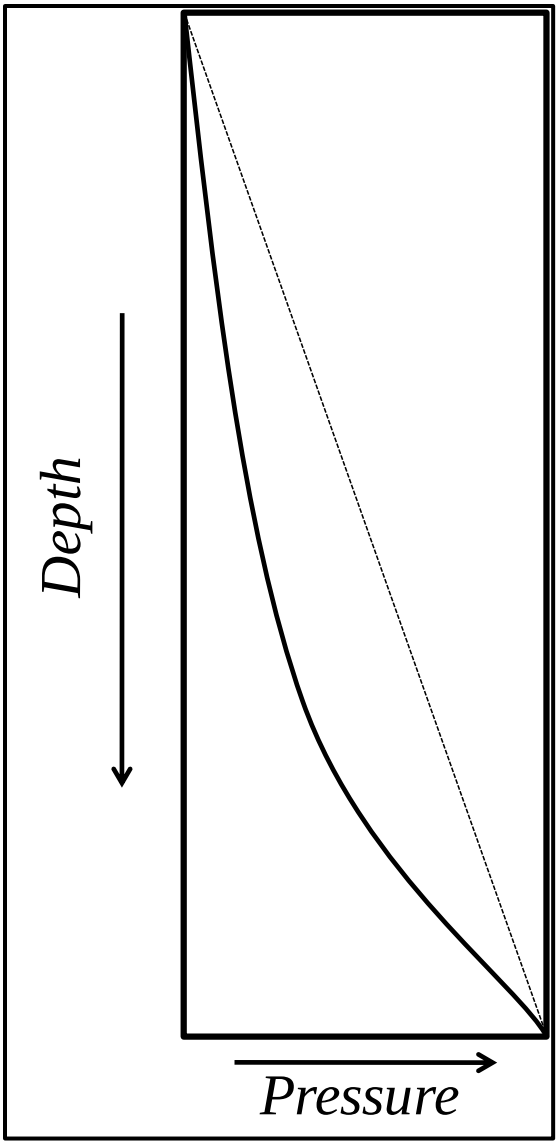

Figure 3.5 – Hydrostatic Pressure Profile in Gas Column.

During the formation of the oil column beneath the gas, as oil from the upper sections of the well moves downward, some liberated gas dissolves back into the oil. Conversely, as oil from the lower sections moves upward, solution gas would be liberated. Since, the column of oil would be formed between the gas and water (in the middle of the well),

these two opposite effects could be ignored. Nevertheless, since the solution gas content and oil density vary throughout the column of oil, the hydrostatic pressure should not be averaged over the length of the column. Dividing the oil column into number of segments and adding up the hydrostatics of each, would be a sensible way to calculate the $P_{oil\ column}$ in **Eq. 3.8**.

Note that, when the well is shut-in, in addition to the pressure rise caused by the formation of the gas cap, the BHP also increases with the reservoir's pressure build-up. Reservoirs with strong aquifer are examples of fast BHP recovery. In the short term shut-in analysis described above, it is recommended to use the predicted future reservoir pressure as the current BHP to avoid underestimation of the pressure at the bottom of the well.

3.2.1.1 Bubble Rise Velocity

The formation of gas bubble and its subsequent buoyancy driven rise is a very important fundamental phenomenon that contributes significantly to the hydrodynamics in shut-in analysis. In dispersion systems, the rise of a bubble can be associated with possible coalescence and dispersion followed by disengagement.

The rise of a gas bubble in liquid systems is a function of several parameters including, bubble size and shape, properties of gas-liquid systems (density, viscosity, surface

tension), liquid motion direction, and operating conditions (temperature, pressure, gravity). Normally, gas bubbles experience a slip and the presence of viscous and inertial forces makes the analysis complicated. To simplify the case, it is assumed that the fluid surrounding the bubble has zero viscosity, and there is no slip at the boundary.

Since the bubble rise velocity varies with the system properties, many investigators have developed empirical, semi-empirical, and theoretical formulations. Hence, most of the formulations are subjective to a narrow range of governing parameters. Talaia (2008) states that using the fundamental approach based on Stokes' law and simple force balance, for small spherical bubbles, the drag force can be combined with the buoyancy force to yield;

$$V_{bubble\ rise} = \frac{2g(\rho_L - \rho_g)}{9\,\mu_L} R_b^2, \quad \text{..... (3.10)}$$

Where;

g = Acceleration due to gravity, m/ s^2

ρ_L = Liquid density, kg/m^3

ρ_G = Gas density, kg/m^3

μ_L = Liquid viscosity, Pas

R_b = Bubble radius, m

In the past, field personnel have used a gas migration rate of 1000 feet per hour based on a "rule of thumb". Zuber and Findlay (1965) developed a model to estimate the mean gas velocity as;

$$\overline{v_g} = C_0 v_H + v_s, \quad \text{..... (3.11)}$$

Where,

$\overline{v_g}$= Mean gas velocity

v_s= Gas bubble slip velocity

v_H= Homogenous velocity

They proposed that the coefficient C_0 is related to the distribution of the bubbles and their relative velocities across the pipe. By suggesting plausible velocity and void fraction profiles, they showed that C_0 would range from 1.0 to 1.5. According to Johnson and Cooper (1993), the distribution factor is independent of the deviation up to 45° which implies that there is no significant change in the flow field. With further deviation the buoyancy of the bubbles at the top of the• pipe starts to distort the liquid velocity distribution and increase the distribution factor.

Other authors have discussed the rise velocity of isolated bubbles in stationary columns of liquid. Some assumed Stokes flow both around and inside the bubble and some developed correlations to describe the rise of single, slightly larger bubble as function of

density difference and surface tension. Harmathy (1960) developed a correlation independent of bubble size as;

$$v_s = 1.53\left(\frac{g(\rho_L-\rho_G)\sigma}{{\rho_L}^2}\right)^{0.25}, \quad \text{..... (3.12)}$$

Where, ρ_L and ρ_G are liquid and gas densities, respectively, and σ in the Interfacial Tension (IFT). For air and water, the predicted bubble velocity is 150 ft/min.

Davies and Taylor (Johnson and White (1991)) developed a correlation for larger bubbles that almost fill the pipe as;

$$v_s = 0.35\left(\frac{g(\rho_L-\rho_G)d}{\rho_L}\right), \quad \text{..... (3.13)}$$

Where, "d" is the pipe diameter. The correlation is referred to as the "Taylor Bubble" velocity. For air and water flow in a 7.8 inch pipe, the predicted rise velocity is 290 ft/min.

Early studies by Rader et al. (1975) illustrated that the factors affecting the rate of bubble rise include the properties of the influx, mud properties, the eccentricity of the hole, the geometry of the conduit, and the manner in which the influx enters the wellbore. For instance, a dispersed influx migrates much slower than a continuous

bubble. The incremental changes in surface pressure were utilized to determine the rate of rise.

Using the surface pressure rise, pc, Johnson and Tarvin (1993) proposed the following correlation to calculate the slip velocity;

$$p_c = \frac{X_g V_g \rho_m g v_s - q_e}{X_g V_g + X_w V_w + X_m V_m}, \quad \text{..... (3.14)}$$

Where, X_g and V_g are the influx compressibility and volume respectively, X_w and V_w the wellbore compliance and volume and X_m and V_m the mud compressibility and volume. q_e is the fluid loss rate from the wellbore.

Johnson and White (1991) stated that gas will rise faster in a viscous fluid than in water. According to Johnson and Cooper (1993), in a stationary column of mud, the gas normally migrates at a velocity of more than 100 ft/min. However, the estimated gas velocities, derived from shut-in surface pressures are typically around 15 ft/min. To explain this discrepancy, they stated that because of neglecting the effects of mud compressibility, fluid loss, and wellbore elasticity, the conventional field interpretation of the shut-in surface pressure rise is wrong and can underestimate the migration velocity by an order of magnitude. Also, for the air - mud flows in the pipe geometry, deviation increases the slip velocity. The greatest increase is for small deviations. As the pipe angle passes 45°, the slip velocity falls back towards the vertical value.

In an effort to further illuminate the complexity of the gas migration, Grace et al. (1996) documented instances of influx migration under a variety of conditions. In their study, the highest rate of migration was 1339 feet per hour, which was observed in the wellbore inclined to 38 degrees. In the vertical wells, the highest observed migration rate was 784 feet per hour in fresh water. According to the authors, the migration rate can and usually will vary throughout the process and normally, the migration rate will increase as the influx approaches the surface. Authors concluded that the surface pressures could be relied upon to predict influx behavior and migration rate.

Santos and Azar (1997) proposed a correlation that accounts for the non-Newtonian behavior of the wellbore fluid, inclination, and geometry of the wellbore. Their correlation is expressed as;

$$v_b = c_1\, c_2\, c_3 \left(\frac{g(\rho_L - \rho_G)d}{\rho_L}\right), \quad \text{..... (3.15)}$$

Where constant c_1 accounts for the effect of the geometry and for an annuli geometry with "R' being the ratio of the inner and outer diameters, the linear fitting of the experimental data has yielded to;

$$c_1 = 0.3143\, R + 0.2551, \quad \text{..... (3.16)}$$

c_2 accounts for the non-Newtonian behavior of the fluid and could be correlated with the bubble Reynolds number, RN_B. Similar to c_1, the linear fitting of the experimental data has yielded to;

$$c_2 = 0.0532\, Log(RN_B) + 0.7708, \quad \text{..... (3.17)}$$

The correction for the inclination angle, α, is introduced with the c_3 and is defined as;

$$c_3 = 1 + (0.0586\, Log(RN_B) + 0.0042) Sin\,(2\alpha), \quad \text{..... (3.18)}$$

Authors claim that their model shows a very good agreement with experimental data for inclinations as high as 80^o.

The gas migration mechanism for the short term, intermediate term, and long term shut-in analysis is considerably different. As it is shown in **Fig. 3.6**, volume and velocity of the migrating free or liberated gas is different in each case.

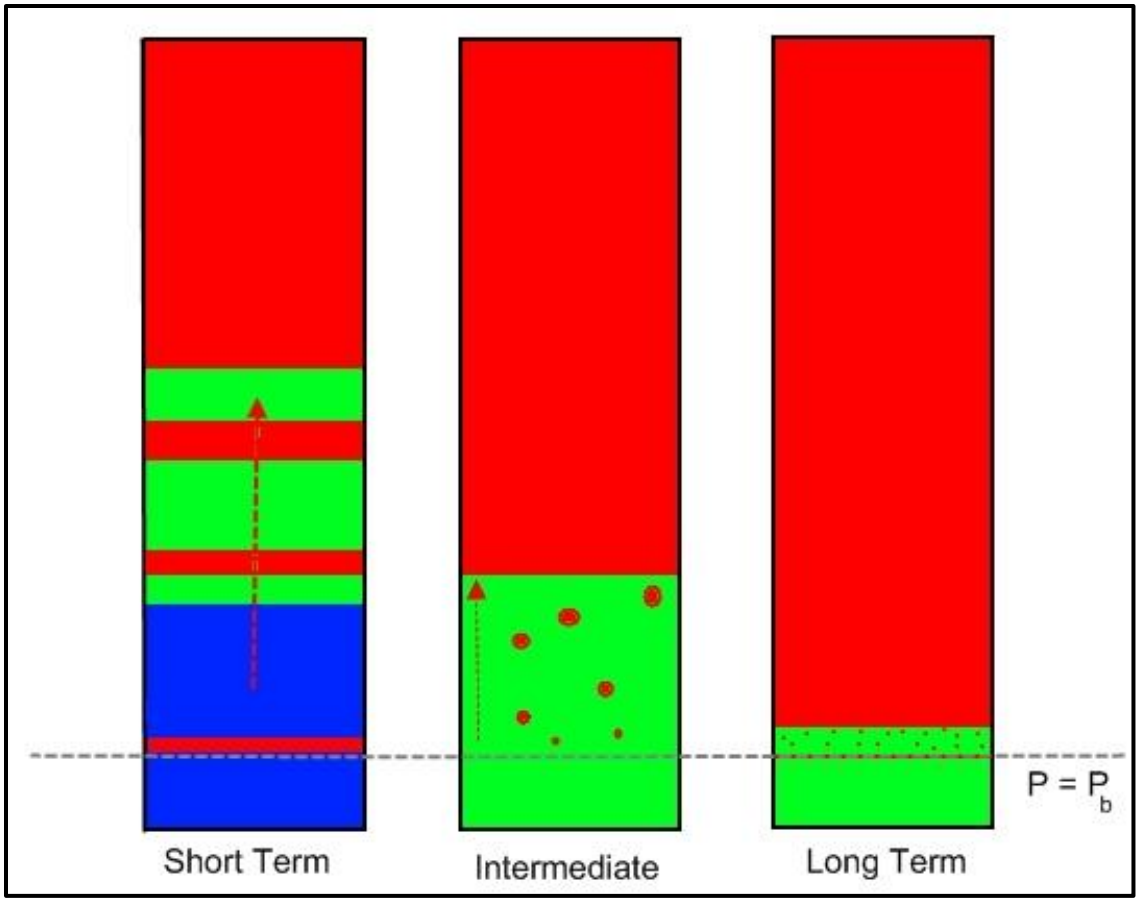

Figure 3.6 – Formation of the Gas Cap During the Shut-in Period. The Gas Volume and Migration Mechanism is Different for Each Shut-in Period.

The gas migration analysis in the short term shut-in is similar to the kick migration. The gas liberation and consequent migration of the gas bubbles during the intermediate period could be modeled with the existing bubble rise models. The gas liberation and percolation during the long term shut-in is a complex phenomenon and there is no existing model to quantify the liberation rate. Hence, in this research, the liberation rate is considered as an input that could be manipulated. It has been suggested that, until further developments, the liberation rate could be expressed as a rate in which the total

volume of the gas increases. Therefore, at a constant geometry, the rate of increase in the length of the gas column is proportional to the rate of gas liberation and could be expressed as feet per day.

Considering the fact that wellbore conditions such as; inclination, temperature, and pressure vary with depth, the wellbore needs to be divided into segments. Then, each segment should be evaluated separately. Therefore, to account for the variations and uncertainties associated with the migration rate, a nominal migration rate is introduced to include all the effects. Note that the main purpose of this study is to estimate the volume and height of the segregated fluids inside the wellbore. Hence, the data acquired through pressure build-up tests are used to back calculate the nominal migration rate. The nominal migration rate is manipulated to match the surface pressure with the test duration.

3.2.2 Application

In well testing, the measurement and analysis of bottomhole pressure data of a shut-in producing well is called a buildup test. Buildup tests are the most common way to determine well flow capacity, permeability, reservoir thickness, skin, and other information. Since, in a buildup test, the well is shut-in for a short period of time (usually 24 hours), the short term shut-in analysis can be used to predict the measured final surface shut-in pressure. In other words, the short term shut-in module and buildup

test interpretations can be used together as a verification method to predict the wellbore conditions. Also, some other key indefinite parameters such as the bubble rise velocity can be approximated with the comparison of the predicted and the measured surface pressure values. Also, the short term shut-in analysis would be the first step in subsequent intermediate term and long term shut-in analysis.

Considering the well conditions described earlier (section 3.1.2), a sample short term shut-in analysis is presented as follows;

According to **Table 3.1**, the surface shut-in pressure after 24 hours buildup test is measured to be 966 psi. First, using the manipulation option, the bubble rise velocity is set to 3.5 ft/min to simulate the shut-in conditions for the same period as the buildup test.

Table 3.1 – Sample Static Pressure Survey

MEASURED DEPTH	WIRELINE DEPTH	MEASURED TVD	PRESSURE PSIG	GRADIENT PSI./FT	TEMPERATURE DEG.F.	GRADIENT DEG.F/FT
69	0	69	966		78	
1069	1000	1069	988	.022	96	.018
2069	2000	2062	1149	.163	109	.013
3069	3000	2989	1483	.359	111	.002
4069	4000	3707	1740	.358	121	.014
5069	5000	4396	1996	.373	130	.013
6069	6000	5121	2313	.437	137	.009
7069	7000	5879	2645	.438	142	.007
7569	7500	6262	2811	.435	146	.009
7969	7900	6573	2947	.437	148	.008
8432	8363	6919	3100	.440	152	.011

As it is shown in **Fig. 3.7**, the predicted surface shut-in pressure is fairly close to the measured value. Consistent with the well trajectory shown in **Fig. 3.7**, the pressure versus time profile is comprised of three distinct slopes, each linked to the pathway of the migrating bubbles.

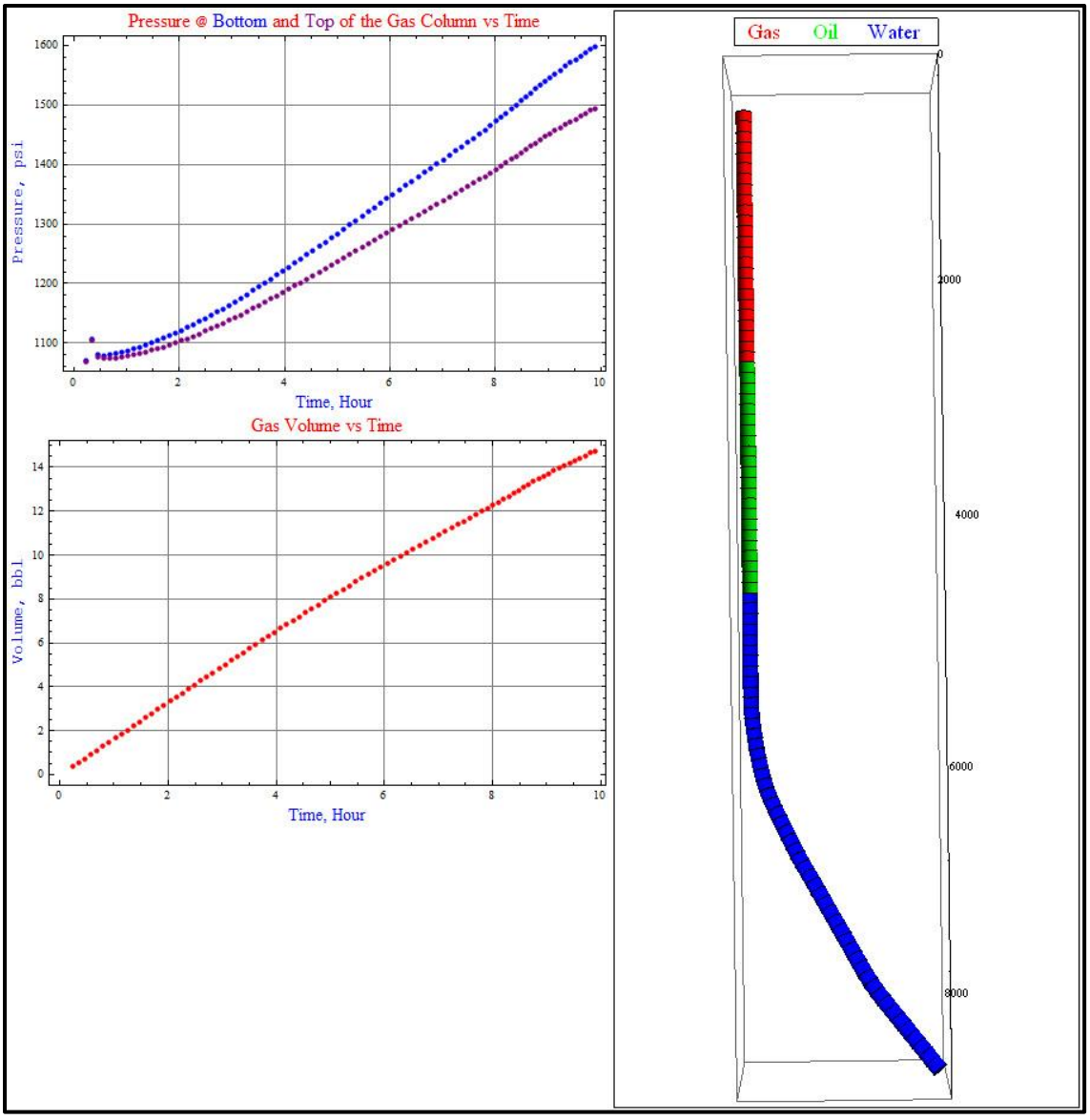

Figure 3.7 –Short Term Shut-In. Surface shut-in pressure profile for the top of the gas cap (purple) and average pressure of the gas cap (blue).

Also in **Fig. 3.7**, the separation and placement of the wellbore, accumulation of the migrating bubbles, and formation of the gas cap over the time are presented**.**

3.3 Intermediate Term Shut-In

After the initial separation of the fluids, it is assumed that the water is pushed back into the reservoir and an equivalent volume of oil plus gas replaces the water. In the meantime, similar to the short term gas migration process, gas continues to migrate toward the created gas column at the upper sections of the wellbore.

3.3.1 Theory

Subsequent to the fluid separation in the first few hours, at the pay zone, the wellbore's contained fluid (water only) has a higher density than the formation's fluid (water + oil + gas). As a result, because of the difference in the densities, water and oil swap sides. Considering the fact that the fluid exchange takes place over the entire pay interval, to determine the overall exchange rate, the average exchange rate over the payzone thickness should be determined.

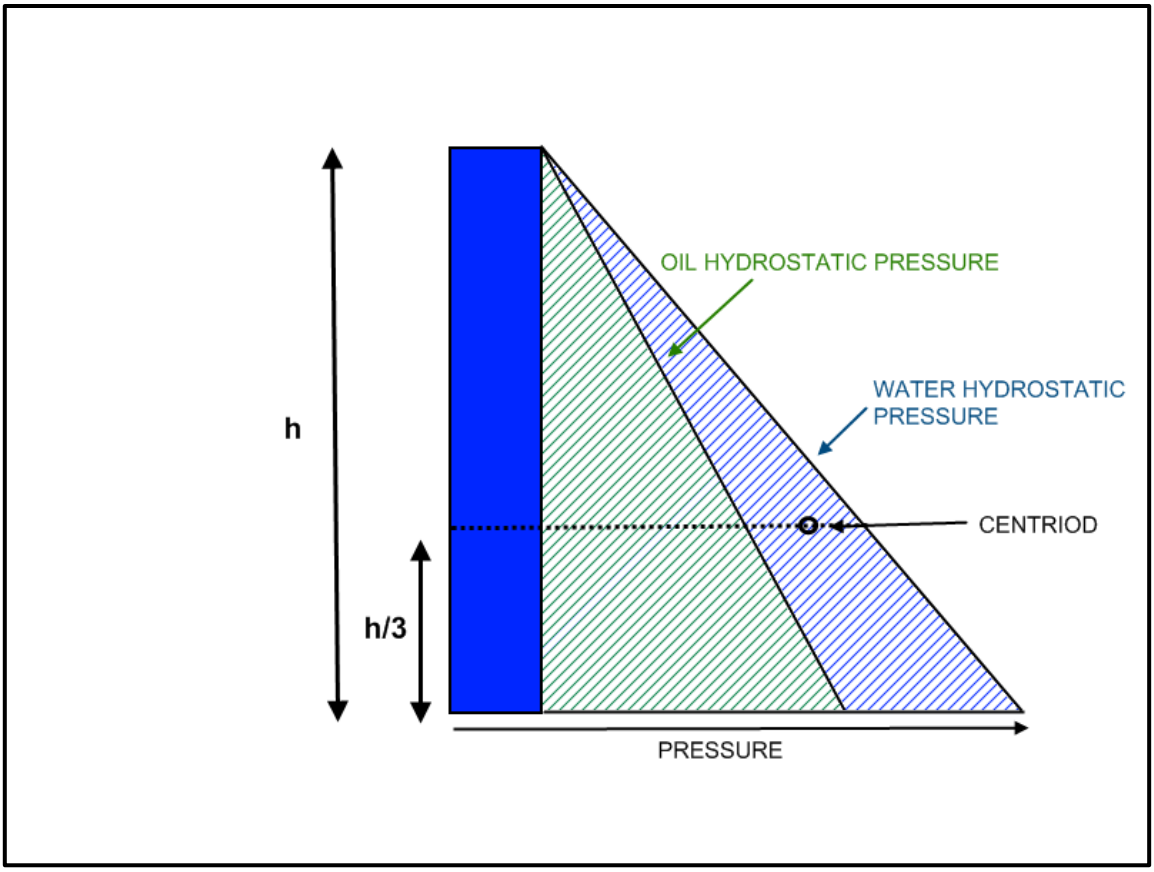

Figure 3.8 – Fluid Exchange Point at the Payzone. At the payzone, the difference in pressures of the fluid columns inside the well (blue) and inside the reservoir (green) causes the fluids to swap places.

To simplify the problem, as it is shown in **Fig. 3.8**, the centroid of a triangle with hydrostatic pressure gradients of each fluid being the vertexes is considered as the fluid exchange position. Consequently, the rate of fluid exchange could be obtained as;

$$Transfer\ rate = 0.052\ (Water\ Density - Oil\ Density)\frac{payzone\ \ TVD}{3}\ J^*\ ,\quad \text{..... (3.19)}$$

Where, the densities are in ppg, the payzone thickness in ft, and J^* is a function of reservoir properties.

The gas migration is simulated using a method much like the short term module. In the case of BHP greater than the bubble point pressure, the volume of the migrating gas would be calculated based on the difference between the oil's solution gas content at the oil and gas interface and where the oil column pressure equals the bubble point pressure.

3.3.2 Application

Depending on reservoir characteristics such as permeability and skin, after a certain period of time, the hydrocarbon content and the wellhead shut-in pressure could be approximated. Also, the water displacement period that takes place before the final stabilization of the wellbore would be estimated prior to the subsequent long term shut-in analysis. Considering the well conditions described earlier (section 3.2.2), a sample intermediate term shut-in analysis is presented as follows;

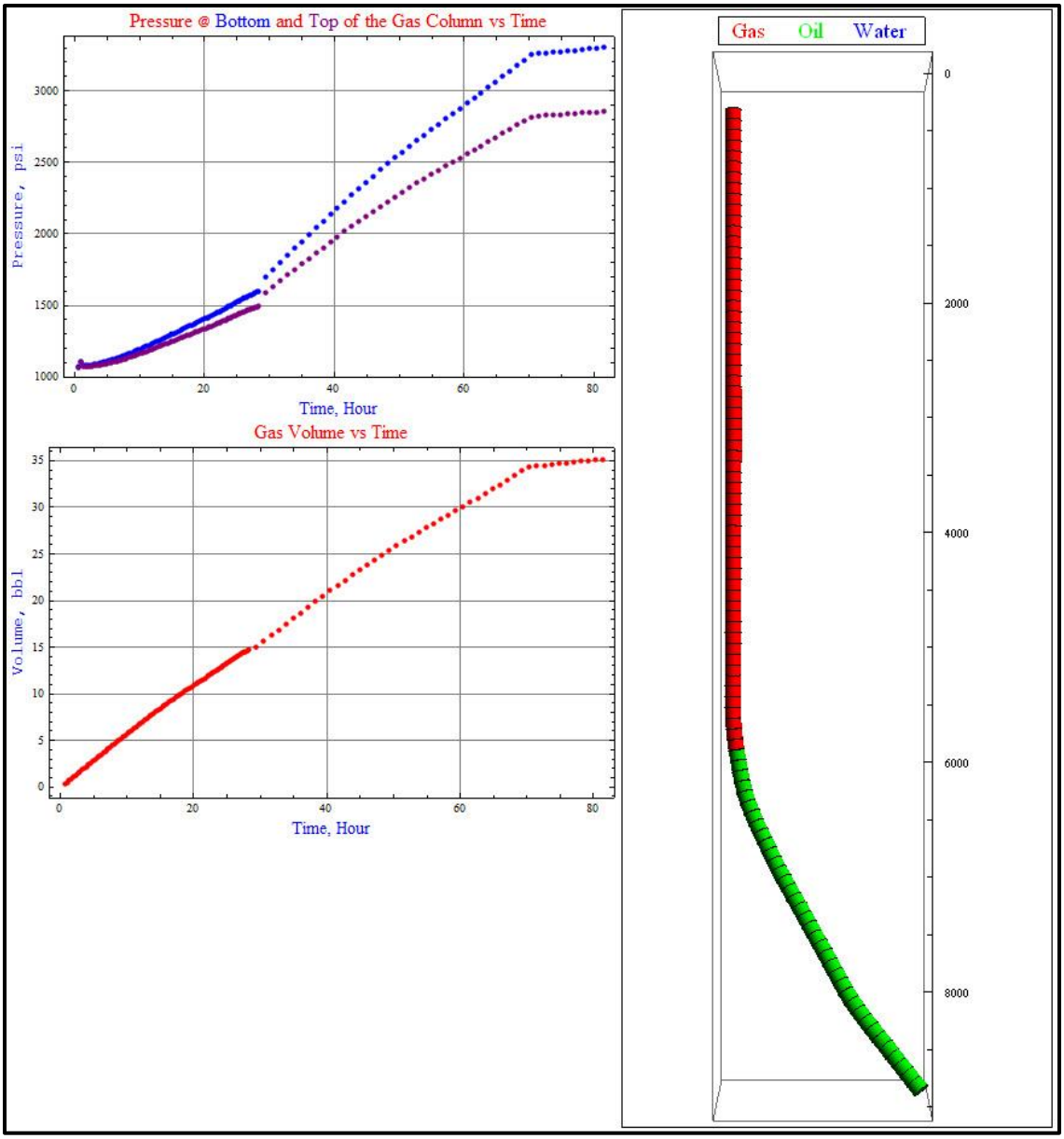

Figure 3.9 – Intermediate Term Shut-In Analysis.

As it is shown in **Fig. 3.9**, after 85 days, all the water is pushed back into the reservoir. Compared to the short term analysis, there is a larger gas column with a higher surface

shut-in pressure. Note that, the change of slope in **Fig. 3.9** corresponds to the time when the pressure at the bottom of the oil column exceeds the bubble point pressure.

3.4 Long Term Shut-In

When oil and gas are the only fluids contained in the wellbore, the stabilization period initiates. At this stage, the liberation and upward migration of the solution gas continues until the time that the pressure at the bottom of the gas column and top of the oil column (oil-gas interface) equals the bubble point pressure. Hence, for undersaturated oil reservoirs, the stabilization period is finished only when the whole wellbore is filled with the gas.

3.4.1 Theory

The general methodology is quite the same as the one used in the previous modules with the only difference being the extent of the solution gas liberation over time. The rate of gas liberation and the pace that the liberated gas reaches the gas-oil interface is a very complex subject. To date, there is not an established study addressing the well stabilization under the long term abandonment. Because of certain uncertainties involved with this phenomenon, the gas percolation over the time is considered as a variable that could be changed by the user. The default value of 10 ft/day is considered to be a reasonable assumption.

3.4.2 Application

Considering the well conditions described earlier (section 3.3.2), a sample long term shut-in analysis is presented as follows;

As it is shown in **Fig. 3.10**, after 215 days, high percentage of the oil is pushed back into the reservoir. Compared to the intermediate term analysis, there is a larger gas column with a higher surface shut-in pressure.

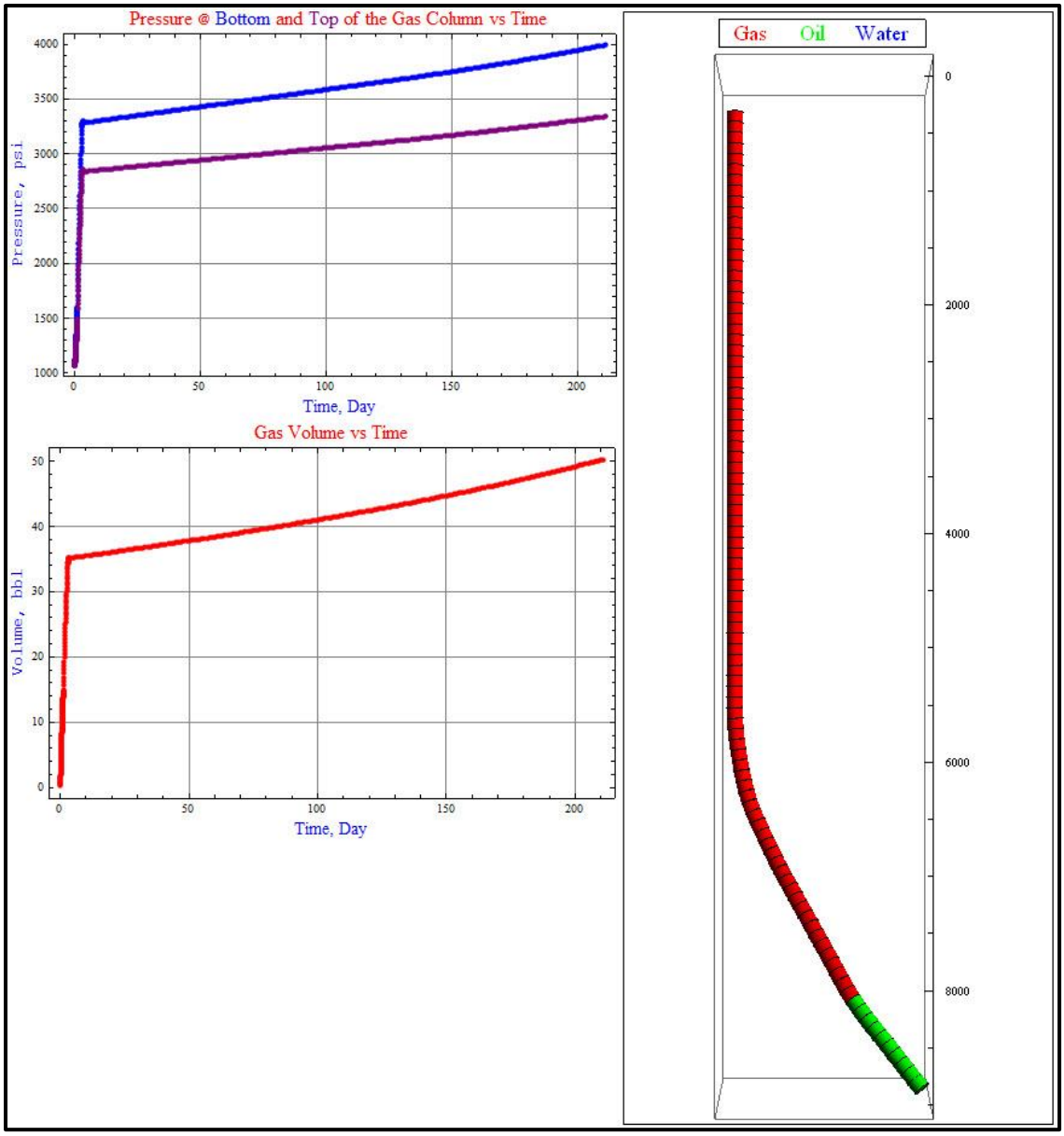

Figure 3.10 – Long Term Shut-In Analysis.

4. MODULE III: PLUGGING SCENARIOS

After achieving the planned intercept and establishing the hydraulic communication with the Target Well (TW), two distinct hydraulic based operations will commence. The initial operation will include a stabilization period to equalize the hydrostatic differences of the fluids in the two wells, followed by the plugging operation. The plugging operation will require the placement of permanent plugging fluids such as cement or resin into the target well. In this section, the dynamics of the plugging fluids placement will be discussed in detail.

According to **Fig. 4.1**, when the plugging fluid enters the TW, depending on where the interception point is, it could flow through several distinct flow paths and directions. In general, the target wells would fall into two well conditions: the well is open to the surface (open system) and the well is not open to the surface (closed system). Based on the condition above and below the interception point, accounting for the hydrostatics, frictional losses, and any other sort of resistance to the flow, the injected fluid could flow in upward direction, downward direction, or combination of the two. Furthermore, depending on the wellbore geometry, the plugging fluid may flow in annular flow path, tubular flow path, or combination of both.

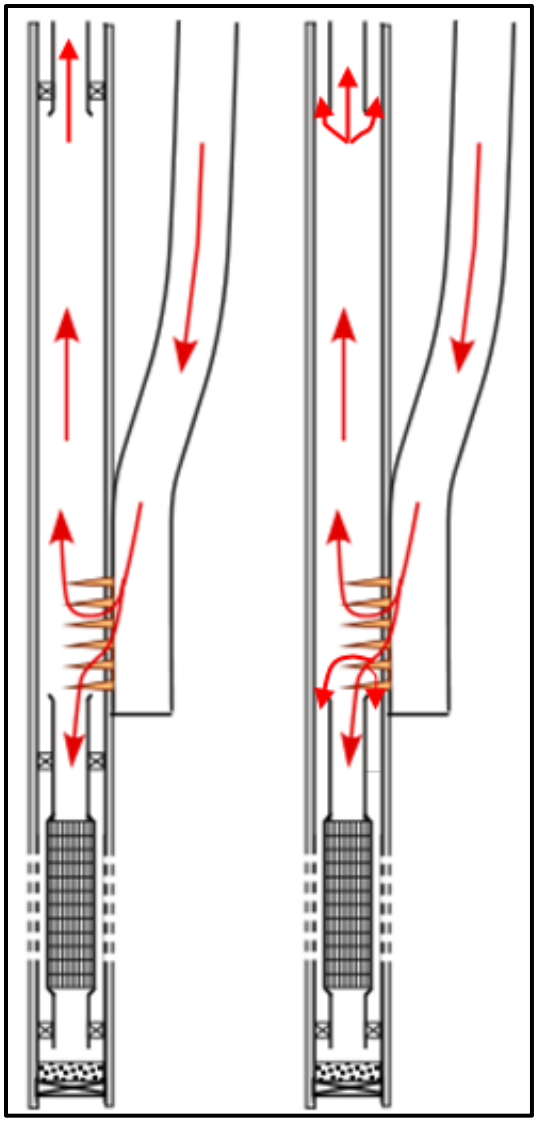

Figure 4.1 – Flow Direction and Flow Type vs. Completion. In addition to the direction of the flow, depending on the completion type, the plugging material may flow in tubular area, annular area or both. The flow area would affect the required volume and frictional losses.

The desired interception scenario, as depicted in **Fig. 4.2**, could be selected with setting the appropriate built-in radio buttons. The density and rheological properties of the plugging fluid along with those of any other fluid whether injected or initially present,

both IW and TW geometries, fracture gradients, and perforation details are some of the essential input data for the plugging operations analysis.

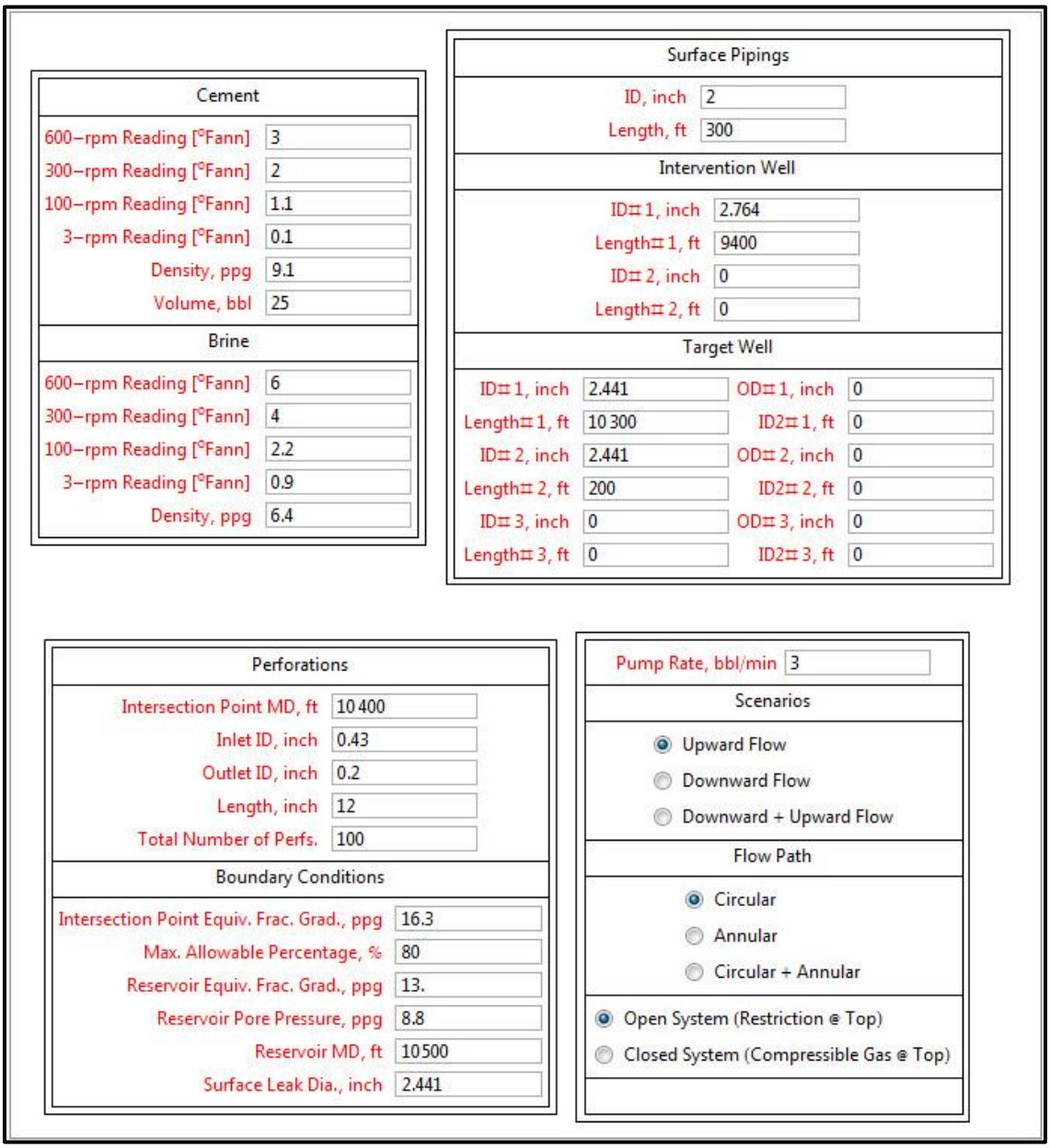

Figure 4.2 – The Plugging Scenarios.

Since, during pumping of the plugging material into the target well, the pump rate and pressure are the only parameter that could be monitored the pump pressure, as the base node, is plotted versus pumped volume (or pumping time). Note that, pumping at a constant rate would help to detect the changes in geometry and flow regions. Thus, the hydraulics of the flowing plugging fluid is traced through the surface piping, IW, perforations, and into the TW.

4.1 Surface Piping

Setting the pump as the base pressure node, the plugging fluid will first flow through the surface piping to get to into the IW. It is assumed that a low viscosity fluid such as brine or spacer is pumped ahead and behind the more viscous plugging material. Therefore, the entrance and the exit of the plugging material into and out of the surface piping should be evident in the pump pressure plot. Since there would be negligible change in elevation, the frictional pressure loss is determined on the basis of rheological properties, pump rate, length and diameter of the surface piping. The pressure loss through this section can symbolically be written as;

$$\Delta P_{SP} = f[\{q, d_i, L, \mu\}]_{frictiona\ l\ loss}, \quad \text{..... (4.1)}$$

Where;

ΔP_{sp} = Surface piping total pressure change

q = Pump rate

d_i = Inner diameter

L = Length

μ = Viscosity

Also, $f[x]_{frictional\ loss}$ is defined in Appendix C. Note that, at constant rate, based on the volume of the pumped plugging fluid, ΔP_{sp} fluid viscosity should be updated with the time. Likewise, in addition to the viscosity, the changes in the density will be taken into account for the rest of the wellbore sections.

4.2 Intervention Well (IW)

While, the outflow of the surface piping section would be the inflow to the IW, the hydraulics inside the IW is to be computed next. Inside the IW, the pressure change with regard to the pump is given by;

$$\Delta P_{IW} = f[\{q, d_i, L, \mu\}]_{frictional\ \ loss} - f[\{\rho, Z\}]_{hydrostatic}\ , \quad \text{..... (4.2)}$$

Where;

ΔP_{IW} = Intervention well total pressure change

Z = Vertical change in elevation

ρ = Density

Also, $f[x]_{hydrostatic}$ is defined in Appendix C. Considering the fact that in directional and deviated wells, Measured Depth (MD) is different from the True Vertical Depth (TVD), directional survey data is needed to differentiate between them. Thus, the minimum curvature method is built into the program to process the directional survey data.

To be able to handle the changes in the properties of the contained fluids and also keep track of the pumped plugging fluid, both the IW and TW are divided into 100 ft long segments. Then, each segment is treated as a control volume with the inflow and outflow being respectively the outflow of the previous and inflow to the next segments.

4.3 Perforations

Perforations are the induced communication channels which collectively form the Total Flow Area (TFA) between the IW and the TW. The flow through the perforation is analyzed based on three important characteristics including; number of shots over the perforated interval, length of the channels, and inlet and outlet channel diameters.

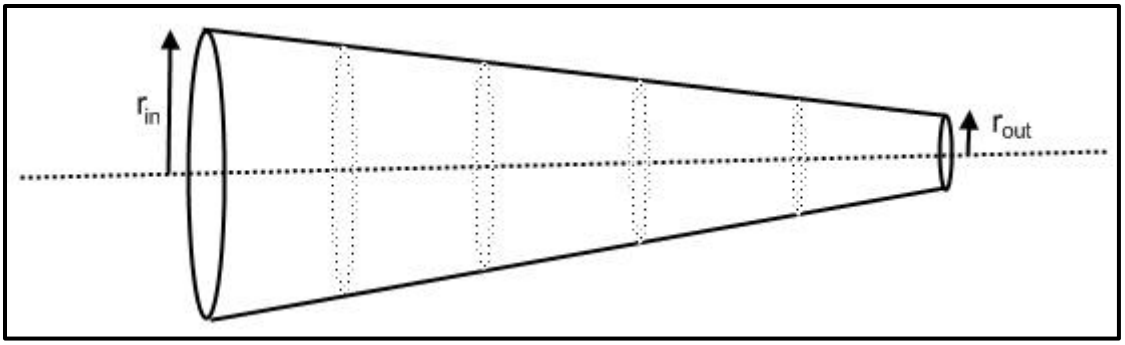

Figure 4.3 – The Perforation Tunnel. Because the radius of the funnel decreases over the length, the entire length is divided into segments. The pressure loss is calculated in each segment and the sum is used as the total loss.

Assuming a cone shaped tunnel (**Fig. 4.3**), the pressure loss through the perforations is presented as;

$$\Delta P_{Perfs} = \sum_{j=1}^{L} f\left[\{q, d_{i_j}, L_j, \mu\}\right]_{frictional\ \ loss}, \quad \text{..... (4.3)}$$

Where;

ΔP_{perfs} = Perforations total pressure change

d_{ij} = Inner diameter as function of length

4.4 Target Well (TW)

The TW hydraulics analysis investigates the flow downstream of the perforations. As discussed earlier, many different flowing scenarios may take place inside the TW. The flow paths below and above the interception point along with the selected system or flow

direction highly affects the TW's hydraulics. Having up to three different geometries, multiple combinations of annular, tubular, or both can be chosen. Clearly, the frictional pressure loss inside the annular path is handled differently from that of the tubular.

4.4.1 Open System

Here, the term "open system", is applied to a well which is to some extent open to the surface. The outflow is modeled with a choke, meaning, any resistance to the flow is represented by the pressure loss through the choke.

Pressure drop across a choke is usually very significant. Varieties of choke flow models are available from the literature, yet there is no universal equation for predicting pressure drop across the chokes. Based on the gas fraction in the fluid and flow regimes, the flow can be categorized into subsonic or sonic. When the fluid velocity in a choke, under in situ conditions, reaches the traveling velocity of sound the flow is called "sonic flow". Under sonic flow conditions, because of the pressure discontinuity at the choke, the downstream pressure is independent of upstream pressure. The existence of the sonic flow depends on "downstream to upstream" pressure ratio. A pressure ratio greater than the critical pressure ratio would generate sonic flow. The critical pressure ratio through chokes is expressed as;

$$\left(\frac{P_{outlet}}{P_{up}}\right)_c = \left(\frac{2}{K+1}\right)^{\frac{K}{K-1}}, \quad (4.4)$$

Where P_{outlet} is the pressure at choke outlet, P_{up} is the upstream pressure, and $K = \frac{C_p}{C_v}$ is the specific heat ratio. The value of K for natural gas is 1.28, hence the critical pressure ratio for natural gas is about 0.55, which is also used for oil flow.

The correlation for a single phase fluid flow across a choke, with a pressure drop caused by kinetic energy change can be represented as;

$$\Delta P_{\text{choke}} = 1.18 \times 10^{-4} \frac{\rho\, q^2}{\left(C_D\, {d_{ch}}^2\right)^2}, \quad (4.5)$$

Where;

ΔP_{choke} = Choke pressure drop, psi

q = Flow rate, bbl/day

C_D = Choke discharge coefficient

d_{ch} = Choke diameter, inch

For single phase gas flow, in addition to the pressure drop across the choke, temperature drop associated with choke flow is an important issue. Assuming an isentropic process, no time for heat transfer (adiabatic) and negligible friction loss (reversible), the equations for subsonic and sonic flow are presented below. Under subsonic flow

conditions, and specific heat ratio of 1.28, gas passage through a choke can be written as;

$$q_{sc} = 2096\, C_D d^2\, \mathrm{P_{up}} \times \sqrt{\frac{\left(\frac{\mathrm{P_{dn}}}{\mathrm{P_{up}}}\right)^{1.56} - \left(\frac{\mathrm{P_{dn}}}{\mathrm{P_{up}}}\right)^{1.78}}{\gamma_g\, \mathrm{T_{up}}}}, \quad \text{..... (4.6)}$$

Where;

q_{sc} = Gas flow rate, Mscf/day

P_{up} = Upstream pressure at choke, psi

P_{dn} = Downstream pressure at choke, psi

Under sonic flow conditions, the maximum reached passage rate can be expressed as;

$$q_{sc} = 458\, C_D d^2\, \mathrm{P_{up}} \times \sqrt{\frac{1}{\gamma_g\, \mathrm{T_{up}}}}, \quad \text{..... (4.7)}$$

4.4.1.1 Upward Flow

Using a similar approach to that used for the IW, accounting for the hydrostatic pressure build up and frictional losses inside the TW and through the choke, the pressure loss with respect to the pump during an upward flow inside the TW is given as;

$$\Delta P_{TW_{upward}} =$$

$$\Delta P_{\mathrm{choke}} + f[\{q, dp_i, dp_o, dc_i, L, \mu\}]_{frictional\ loss} + \quad f[\{\rho, Z\}]_{hydrostatic}\ , \quad \text{..... (4.8)}$$

Where;

dp_i = Pipe inner diameter

dp_o = Pipe outer diameter

dc_i = Casing inner diameter

A sample plot of pump pressure versus pumped volume for upward flow through different flow paths with various choke sizes is shown in **Fig. 4.4**.

The purpose of having the two smaller plots, depicted in **Fig. 4.4**, is to monitor the integrity of the interception and reservoir zone. In **Fig. 4.4**, the interception zone is referred to as “perforation zone”. Normally, the fracture pressure at the perforation zone is different from that of the producing zone (reservoir zone). The dashed green line represents 80% of the actual fracture gradients at those points.

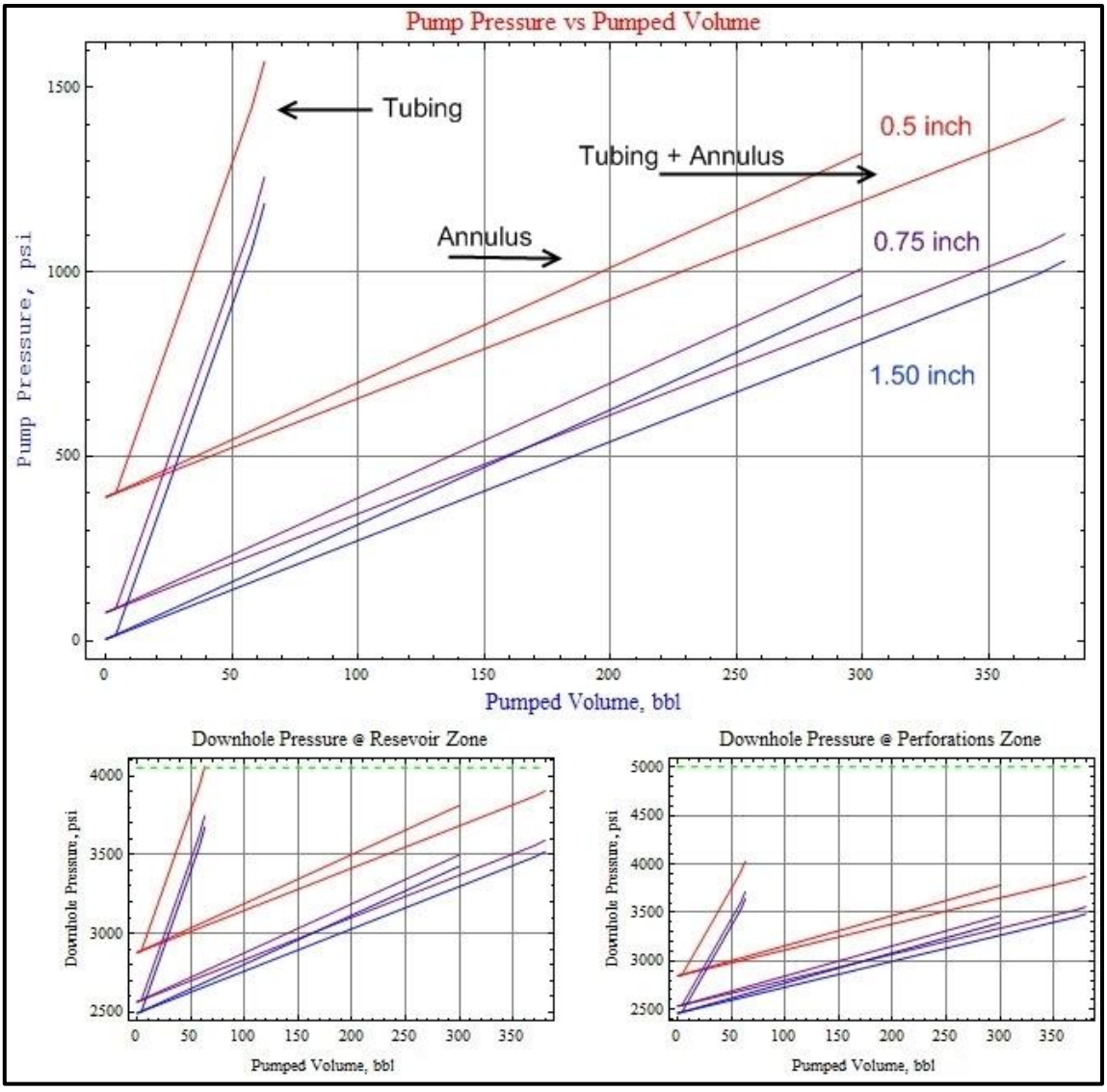

Figure 4.4 – Pressure vs. Pumped Volume Plot for Upward Flow through Tubing, Annulus, and Tubing + Annulus and Choke Sizes of 0.5, 0.75, and 1.5 inch.

4.4.1.2 Downward Flow

In downward flow, as the pumped plugging fluid reaches inside the TW and starts moving toward the producing zone, the existing fluid is pushed back into the reservoir. Hence, similar to the downward flow inside the IW with an additional pressure loss because of the flow through the porous media, the final form is given by;

$$\Delta P_{TW_{downward}} = f[\{q, dp_i, dp_o, dc_i, L, \mu\}]_{frictional\ \ loss} - f[\{\rho, Z\}]_{hydrostatic} + \Delta P_{\text{porous media}}, \quad \text{..... (4.9)}$$

Where;

$\Delta P_{\text{porous media}} = \frac{141.2\ q\ B_o\ \mu_o \left(\ln\frac{r_e}{r_w}+S\right)}{k\ h}$ (see **Eq. 2.7**)

It should be noted, it is assumed that the viscous plugging fluid would not flow into the porous media. As the plugging fluid reaches the payzone, the system should be treated as a closed system. Hence, any further pumping of the plugging material, similar to the LOT, would pressurize the system by simultaneous expansion of the wellbore and compression of the contained fluids. Thus, *the* $\Delta P_{porous\ media}$ should be substituted by the pressure change based on the assumed bulk modulus of 250,000 psi for the oil.

A sample plot of pump pressure versus pumped volume for downward flow with various reservoir permeabilities is shown in **Fig. 4.5**.

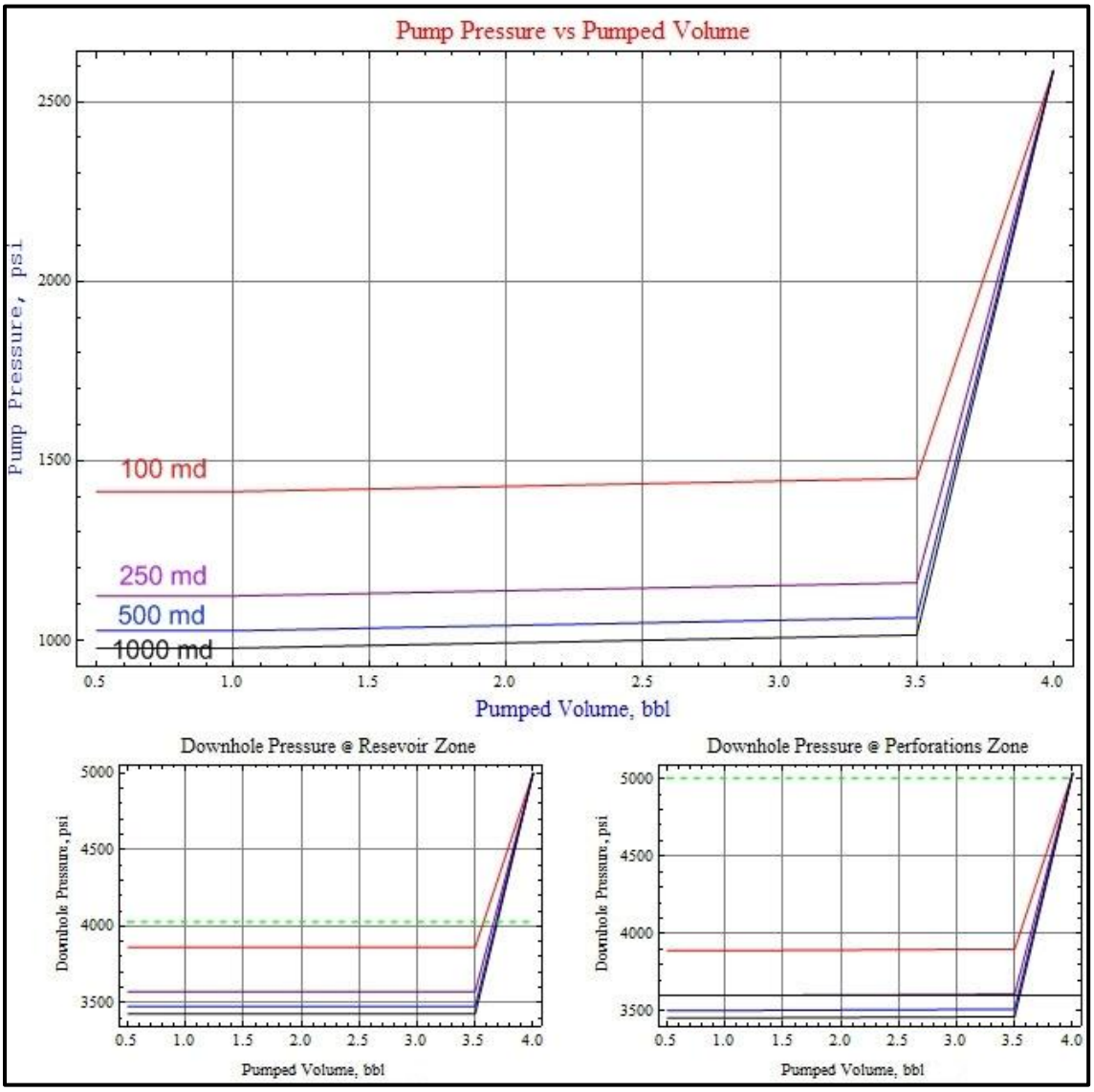

Figure 4.5 – Pressure vs. Pumped Volume Plot for Downward Flow with Permeability Values of 100, 250, 500, and 1000 md.

4.4.1.3 Upward + Downward Flow

An alternate to the assumption of having upward flow only or downward flow only is to assume that the fluid is flowing in both directions at the same time. Then, the fraction of the upward flowing fluid would be determined based on the prevailing conditions. To achieve that, at interception point downstream of the perforations, the fraction at which the upward and downward forces are balanced can be determined by;

$$x_i\left(\Delta P_{\text{choke}} + f[\{q, dp_i, dp_o, dc_i, L, \mu\}]_{frictional\ \ loss} + f[\{\rho, Z\}]_{hydrostatic}\right) =$$

$$(1 - x_i)\left(f[\{q, dp_i, dp_o, dc_i, L, \mu\}]_{frictional\ \ loss} - f[\{\rho, Z\}]_{hydrostatic} + \right.$$

ΔPporous media, ... (4.10)

Where, x_i, is the fraction of the flow that is moving upward. At any step, such as a specified volume entering the TW, **Eq. 4.10** is solved to determine the fraction of the flow going in either direction.

A sample pump pressure versus pumped volume plot for the combination flow is presented in **Fig. 4.6**. Also, each segment of the plot is tagged with its flow area.

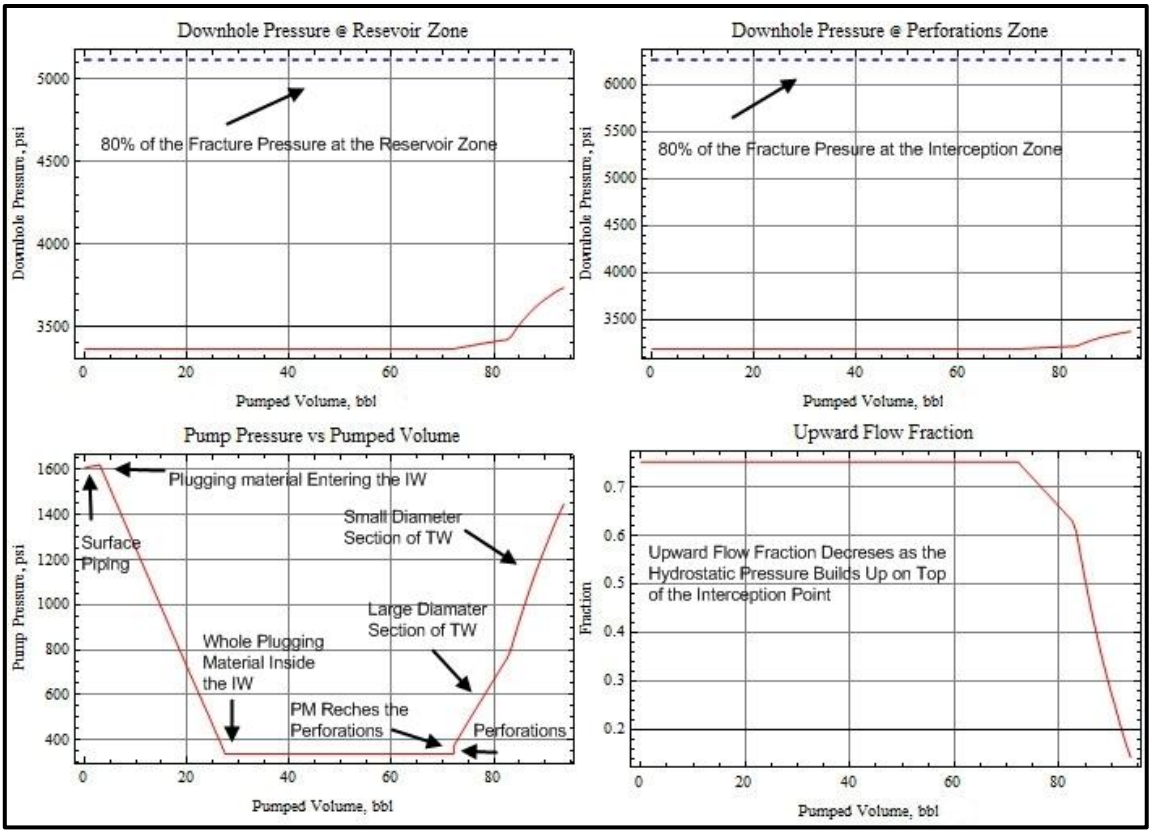

Figure 4.6 – Pressure vs. Pumped Volume Plot for Combination Flow.

4.4.2 Close System

The closed system well is a well which is in static condition and its contents are isolated within the wellbore. Normally, from the operation point of view, it is not feasible to inject large volumes into a closed system well. However, in a case of the existence of a compressible fluid such as gas inside the well, considering the pressurizing limits, the plugging material could be injected into such systems.

In a case of a closed system filled with a compressible fluid such as gas, the injected plugging fluid will compress the gas up the point that the gas could not be compressed any further without exceeding the pressure limitations of the wellbore or formation. Assuming an adiabatic system, the change in the pressure could be written as;

$$P_2 = \frac{P_1 V_1 z_1}{V_2 z_2}, \quad \text{..... (4.11)}$$

Where;

V_1 = Initial volume of the gas

$V_2 = V_1$ - volume of the pumped plugging fluid

Using P_2 as the new average pressure in the column of the gas, then BHP is given as;

$$BHP = P_2 + \frac{1}{2} P_{gas\ column\ \ hydrostatic} + 0.052\ (\rho_{pf} - \rho_o) h_{pf} + 0.052\ \rho_o\ h_o, \quad \text{.. (4.12)}$$

Where;

ρ_{pf} = Density of the plugging fluid, ppg

ρ_o = Density of the oil, ppg

h_{pf} = Height of the column of the plugging fluid, ft

h_o = Height of the column of the oil, ft

Note that, because the plugging fluid is pumped into the closed system at a very slow rate, the frictional pressure losses can be ignored. An example of the pressure versus pumped volume trend for upward flow in a closed system with different gas volumes contained in the wellbore is presented in **Fig. 4.7**. Note that, the gas volume of 25% means that 25% of the volume of the appropriate portion of the wellbore is occupied with gas.

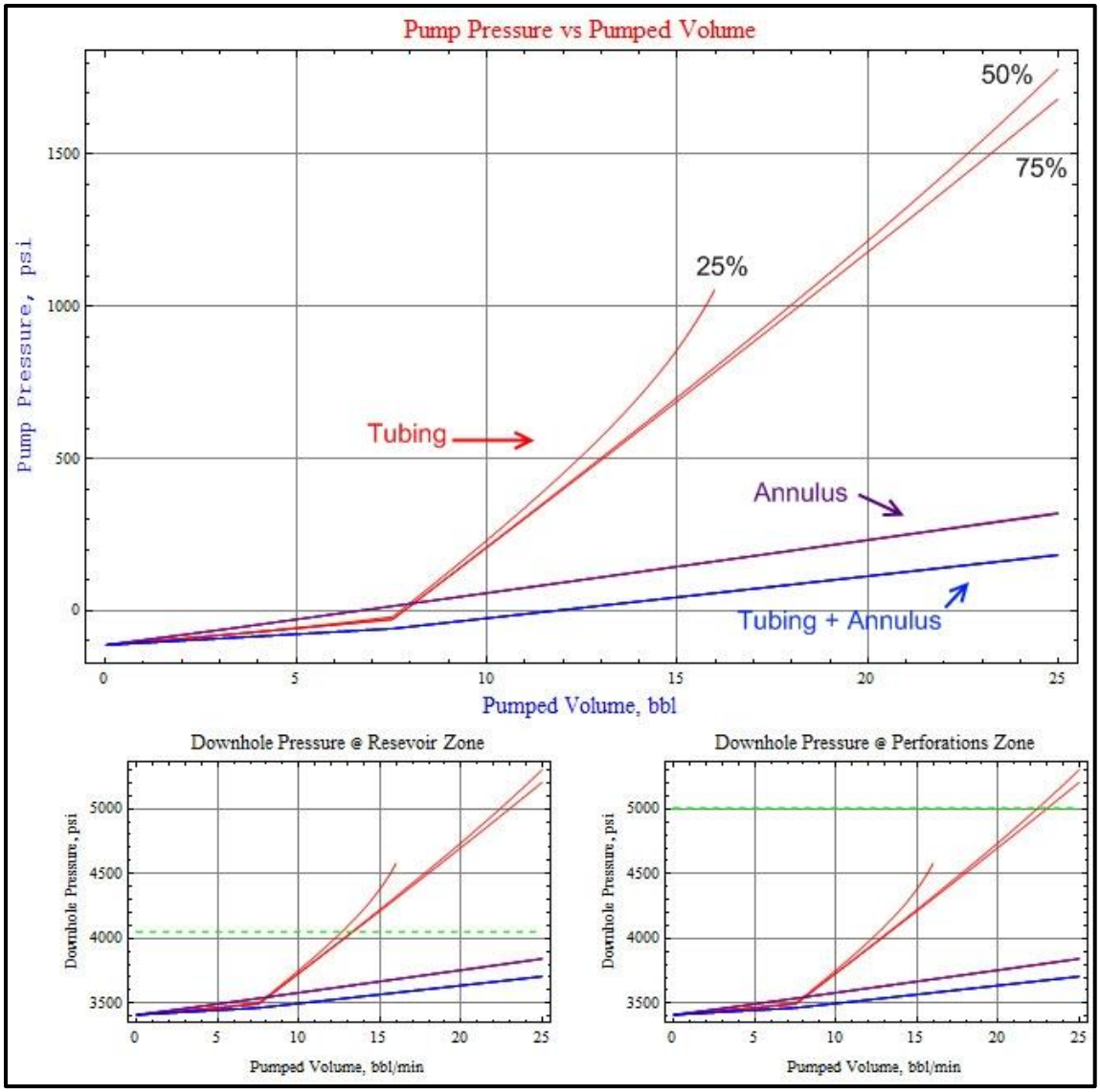

Figure 4.7 – Pressure vs. Pumped Volume Plot for Upward Flow through Tubing, Annulus, and Tubing + Annulus and Gas Percent Volumes of 25%, 50%, and 75% inch.

5. SUMMARY AND CONCLUSIONS

A software package specially designed to analyze and simulate the well intervention hydraulics has been presented. The well intervention toolkit will be used to investigate the plugging and abandonment scenarios. Also, a state-of-the-art inflow performance relationship code in conjunction with a nodal analysis code allows for comprehensive sensitivity analysis of the target well flow dynamics.

The well intervention toolkit provides the following information:

1. Inflow Performance Curves (IPR), reservoir properties such as permeability, porosity, and drainage area, and wellbore conditions such as skin, payzone thickness, and flowing wellbore pressure.
2. Nodal analysis can be performed based on two scenarios; 1) base pressure node at the surface, 2) base pressure node at the bottom of the well.
3. Fluid density requirements in the Intersection Well (IW) to insure well control is maintained after establishing hydraulic communication.
4. Sensitivity analysis of various fluids, densities, intersection depths, and reservoir conditions.
5. Detailed plugging operations characteristics at varying well conditions.
6. Required minimum Total Flow Area (TFA) between the two wells at the intersection point.

7. Sensitivity analysis of plugging materials, placement heights, reservoir conditions in addition to comments on the prediction of the TW fluid compositions in the production tubing and annulus.

Also, it could provide information to make recommendations for achieving a safe and successful intersection and plugging of target wells, along with development of the hydraulic intersection and plugging plan.

5.1 Future Work

Considering the fact that most of the features and application included in the package have never been developed before, it is essential to validate the models with their applications. The performance and accuracy of the toolkit should be tested with actual field data.

Moreover, in order to be able to use the toolkit on variety of cases, the software has been written to make it as generally applicable as possible. However, because of the unique nature of each case, continuous modifications and upgrades are inevitable.

There is a need for further research on gas liberation rate during the long term shut-in period. Furthermore, some additional applications such as dynamic kill, loss to the

adjacent well, dual perforations, and snubbing are either currently under development or in the future development plan.

REFERENCES

Ahmed, T. ed. 1989. *Hydrocarbon Phase Behavior*, Houston: Gulf Publishing Company.

Al-Marhoun, M.A. 1988. Pressure-Volume-Temperature Correlations for Saudi Crude Oils. *JPT* **40** (5): 650-666. SPE-13718-PA.

Brill, J.P. and Beggs, H.D. ed. 1978. *Two-Phase Flow in Pipes*, Tulsa, Oklahoma: The University of Tulsa Press.

Carr, N.L., Kobayashi, R., and Burrows, D.B. Viscosity of Hydrocarbon Gases under Pressure. 1954. *Trans.*, AIME **201**: 264–272.

Economides, M., Hill, A.D., Ehlig-Economides, C. ed. 1993. *Petroleum Production Systems*, Upper Saddle River, New Jersey, Prentice Hall PTR.

Glaso, O. 1980. Generalized Pressure-Volume-Temperature Correlations. *JPT* **32** (5): 785-795. SPE-8016-PA.

Grace, R.D. and Shursen, J.L. 1996. Field Examples of Gas Migration Rates. Paper 35119 presented at the IADC/SPE Drilling Conference, New Orleans, 12-15 March.

Guo, B., Lyons, W.C., Ghalambor, A. ed. 2007. *Petroleum Production Engineering - A Computer Assisted Approach*, Burlington, MA, Elsevier Science & Technology Books.

Hanafy, H.H., Macary, S.M., ElNady, Y.M., Bayomi, A.A., El Batanony, M.H. 1997. A New Approach for Predicting the Crude Oil Properties. Paper SPE 37439

presented at the SPE Production Operations Symposium, Oklahoma City, Oklahoma, 9-11 March.

Harmathy , T.Z. 1960. Velocity of Large Drops and Bubbles in Media of Infinite or Restricted Extent, *AIChE J.* **6**(June): 281-288.

Johnson, A.B. and White, D.B. 1991. Gas-Rise Velocities During Kicks. *SPEDE* (December): 257-263.

Johnson, A.B. and Cooper, S. 1993. Gas Migration Velocities During Gas Kicks in Deviated Wells. Paper 26331 presented at the Annual Technical Conference and Exhibition, Houston, 3-6 October.

Johnson, A.B. and Tarvin, J.A. 1993. Field Calculations Underestimate Gas Migration Velocities. Presented at the IADC European Well Control Conference, Paris, France, 3-5 June.

Petrosky Jr., G.E., Farshad, F.F. 1993. Pressure-Volume-Temperature Correlations for Gulf of Mexico Crude Oils. Paper SPE 26644 presented at the SPE Annual Technical Conference and Exhibition, Houston, 3-6 October.

Rader, D.W., Burgoyne, A.T., Ward, R.H. 1975. Factors Affecting Bubble Rise Velocity of Gas Kicks. *JPT* **27**(5): 571-585.

"Recommended Practice on the Rheology and Hydraulics of Oil-Well Drilling Fluids," Recommended Practice 13D, fifth edition, Washington, D.C. (1 June 2006).

Santos, O.L.A and Azar. J.J. 1997. A Study on Gas Migration in Stagnant Non-Newtonial Fluids. Paper 39019 presented at the Fifth Latin American and Caribbean

Petroleum Engineering Conference and Exhibition, Rio de Janeiro, Brazil, 30 August - 3 September.

Standing, M.B. 1947. A Pressure-Volume-Temperature Correlation for Mixtures of California Oil and Gases. *Drill. & Prod. Prac.* API, 275-287.

Talaia, M. Terminal Velocity of a Bubble Rise in a Liquid Column, *Proc.*, *World Academy of Science, Engineering, and Technology*, **30**. July 2008.

Vasquez, M.E., Beggs, H.D., 1980. Correlations for Fluid Physical Property Prediction. *JPT* (June), 968– 970.

Velarde, J., Blasingame, T.A., McCain Jr., W.D., 1999. Correlation of Black Oil Properties at Pressures below Bubble Point Pressure - A New Approach. *J. Cdn. Pet. Tech.* **38**(13), 62–68.

Vogel, J.V. 1968. Inflow Performance Relationships for Solution Gas Drive Wells. *JPT* **20** (1): 83–92. SPE-1476-PA.

Zuber, N. and Findlay, J.A. 1965. Average Volumetric Concentration in Two-Phase Flow Systems J. Heat Transfer **87**(November): 453-468.

APPENDIX A

Considering the fact that oil composition varies with the region where it originated, a wide variety of PVT models have been developed to correlate crude oil's interrelated properties. Some of the most common correlations are presented as follows;

A.1 Al-Marhoun Correlations

The Al-Marhoun (1985) correlations contain equations for estimating bubble point pressure, solution gas-oil ratio and oil formation volume factor for Saudi Arabian oils. The correlations were developed based on data obtained from 75 bottom hole fluid samples from 62 reservoirs in Saudi Arabia. According to Al-Marhoun, the average errors were lower with the Al-Marhoun correlation than with the Standing and Glaso correlations for Saudi Arabian crude oils. The bubble point pressure is defined as;

$$P_b = -64.138910 + 0.702362 \times 10^{-2}\, X - 2.278475 \times 10^{-9}\, X^2, \quad \text{.....(A.1)}$$

Where;

$$X = R_s^{0.722569}\ \gamma_g^{-1.879109}\ \gamma_o^{3.046590}\ T^{1.302347}, \quad \text{.....(A.2)}$$

And the solution gas-oil ratio is expressed as;

$$R_s = \left(\frac{X}{\gamma_g^{-1.879109}\ \gamma_o^{3.046590}\ T^{1.302347}}\right)^{1/0.722569}, \quad \text{.....(A.3)}$$

Where;

$$X = \frac{-b + \sqrt{b^2 - 4ac}}{2a}$$

$$a = -2.278475 \times 10^{-9}$$

$$b = 0.702362 \times 10^{-2}$$

$$c = -64.138910 - P$$

And oil formation volume factor for saturated oil is presented as;

$$B_o = 0.574095 + 7.723532 \times 10^{-4}\ T +$$

$$2.454005 \times 10^{-3}\ Y + 3.727676 \times 10^{-3}\ Y^2, \quad \text{.....(A.4)}$$

Where;

$$Y = R_s^{0.501538}\ \gamma_g^{-0.145526}\ \gamma_o^{-5.220726}, \quad \text{.....(A.5)}$$

For unsaturated oil;

$$B_o = B_{ob}\ EXP\big(c_o(P_b - P)\big), \quad \text{.....(A.6)}$$

The oil compressibility, c_o, used in **Eq. A.6**, is obtained from the Vasquez and Beggs correlation. Note that, the temperature values, T, used in all equations should be in ^oR.

A.2 Glaso Correlations

The Glaso (1980) correlations contain equations for estimating bubble point pressure, solution gas-oil ratio and oil formation volume factor for North Sea oils. It is stated that the correlations should be valid for all types of oil and gas mixtures after correcting for non-hydrocarbons in the surface gases and the amount of paraffin in the oil. According to Glaso, correlations give a better estimate of oil properties of North Sea oils when compared to the Standing correlations. The bubble point pressure is defined as;

$$P_b = 10^{\left(1.7669+1.7447\ \log X-0.30218\ (\log X)^2\right)}, \quad \text{.....(A.7)}$$

Where;

$$X = \left(\frac{R_s}{\gamma_g}\right)^{0.816} \frac{T^{0.172}}{API^{0.989}}, \quad \text{.....(A.8)}$$

And the solution gas-oil ratio is expressed as;

$$R_s = \left(\frac{X\ API^{0.989}}{T^{0.172}}\right)^{\left(1/0.816\right)} \cdot \gamma_g, \quad \text{.....(A.9)}$$

Where;

$$X = 10^{\left(\frac{-b+\sqrt{b^2-4ac}}{2a}\right)}$$

$$a = -0.30218$$

$$b = 1.7447$$

$$c = 1.7669 - \log P$$

And oil formation volume factor for saturated oil is presented as;

$$B_o = 1 + 10^{\left(-6.58511 + 2.91329 \log Y - 0.27683 (\log Y)^2\right)}, \quad \text{.....(A.10)}$$

Where;

$$Y = \left(\frac{R_s}{\gamma_g}\right)^{0.526} + 0.968\, T\,, \quad \text{.....(A.11)}$$

For unsaturated oil;

$$B_o = B_{ob}\ EXP\big(c_o(P_b - P)\big), \text{.....(A.12)}$$

The oil compressibility, c_o, used in **Eq. A.12**, is obtained from the Vasquez and Beggs correlation. Note that, the temperature values, T, used in all equations should be in ^{o}F.

A.3 Hanafy et al. Correlations

The Hanafy *et al*. (1997) correlations contain equations for estimating bubble point pressure, solution gas-oil ratio, formation volume factor, compressibility, and density for Egyptian oils. The correlations are independent of oil gravity and reservoir temperature. The bubble point pressure is defined as;

$$P_b = 3.205\, R_s + 157.27, \quad \text{.....(A.13)}$$

And the solution gas-oil ratio is expressed as;

$$R_s = -49.069 + 0.312\, P, \quad \text{.....(A.14)}$$

And oil formation volume factor for saturated oil is presented as;

$$B_o = 0.0006\, R_s + 1.079, \quad \text{.....(A.15)}$$

For unsaturated oil;

$$B_o = B_{ob}\, EXP\big(c_o(P_b - P)\big), \quad \text{.....(A.16)}$$

The oil compressibility used in **Eq. A.16**, is obtained from the Vasquez and Beggs correlation.

The density for saturated oil in metric units (grams/cc) is presented as;

$$\rho_{ob} = \frac{1}{2.366 - \frac{1.358}{B_{ob}}}, \quad \text{.....(A.17)}$$

For undersaturated;

$$\rho_{ou} = \rho_{ob}\ EXP\big(c_o(P - P_b)\big), \quad \text{.....(A.18)}$$

The compressibility correlation for saturated oil uses only the oil density at the bubble point. Therefore, the oil compressibility is constant for pressures greater than the bubble point.

$$c_o = EXP\left(\left(\frac{2.582}{\rho_{ob}}\right) - 0.99\right) \times 10^{-6}, \quad \text{.....(A.19)}$$

A.4 Petrosky and Farshad Correlations

The Petrosky and Farshad (1993) correlations contain equations for estimating bubble point pressure, solution gas-oil ratio, formation volume factor, and compressibility for

Gulf of Mexico oils. Petrosky and Farshad state that their correlations provide improved results over other correlations for the Gulf of Mexico, including those published by Standing, Vasquez and Beggs, Glaso, and Al-Marhoun. The bubble point pressure is defined as;

$$P_b = 112.727\left(\frac{R_s^{0.5774}}{\gamma_g^{0.8439}}10^X - 12.34\right), \quad \text{.....(A.20)}$$

Where;

$$X = 4.561\times10^{-5}T^{1.3911} - 7.916\times10^{-4}API^{1.541}, \quad \text{.....(A.21)}$$

And the solution gas-oil ratio is expressed as;

$$R_s = \left(\left(\frac{P}{112.727} + 12.340\right)\gamma_g^{0.8439}10^X\right)^{1.73184}, \quad \text{.....(A.22)}$$

Where;

$$X = 7.916\times10^{-4}API^{1.541} - 4.561\times10^{-5}\,T^{1.3911}, \quad \text{.....(A.23)}$$

And oil formation volume factor for saturated oil is presented as;

$$B_o = 1.0113 + 7.2046\times10^{-5}\left[{R_s}^{0.3738}\left(\frac{\gamma_g^{0.2914}}{\gamma_o^{0.6265}}\right) + 0.24626\,T^{0.5371}\right]^{3.0936}, \quad \text{.....(A.24)}$$

For unsaturated oil;

$$B_o = B_{ob}\ EXP\big(c_o(P_b - P)\big), \quad \text{.....(A.25)}$$

The compressibility correlation for undersaturated oil is expressed as;

$$c_o = 1.705 \times 10^{-7} {R_s}^{0.69357} \gamma_g^{0.1885}\ API^{0.3272}\ T^{0.6729}\ P^{-0.5906}, \quad \text{.....(A.26)}$$

A.5 Standing Correlations

The Standing (1947) correlations contain equations for estimating bubble point pressure, solution gas-oil ratio, and oil formation volume factor for California oils. The bubble point pressure is defined as;

$$P_b = 18.02\left(\left(\frac{R_s}{\gamma_g}\right)^{0.83} \frac{10^{0.0009\ T}}{10^{0.0125\ API}} - 1.4\right), \quad \text{.....(A.27)}$$

And the solution gas-oil ratio is expressed as;

$$R_s = \left(\left(\frac{P}{18.2} + 1.4\right)\frac{10^{0.0125\ API}}{10^{0.0009\ T}}\right)^{(1/0.83)}, \quad \text{.....(A.28)}$$

And oil formation volume factor for saturated oil is presented as,

$$B_o = 0.972 + 1.47 \times 10^{-4}\left[R_s\left(\frac{\gamma_g}{\gamma_o}\right)^{0.5} + 1.25T\right]^{1.175}, \quad \text{.....(A.29)}$$

For unsaturated oil;

$$B_o = B_{ob}\ EXP\big(c_o(P_b - P)\big), \quad \text{.....(A.30)}$$

The oil compressibility, c_o, used in **Eq. A.30**, is obtained from the Vasquez and Beggs correlation. Note that, the temperature values, T, used in all equations should be in ^oF.

A.6 Vasquez and Beggs Correlations

Vasquez and Beggs (1980) developed generally applicable correlations containing equations for solution gas-oil ratio, formation volume factor, and compressibility. The correlations were developed from 600 laboratory PVT analyses from fields all over the world. The data used in the development of the correlations are applicable over wide ranges of pressures and temperatures. Equations are divided into two divisions made at an oil gravity of 30^o API. The bubble point pressure is defined as;

$$P_b = \left[\frac{R_S}{C_1\ \gamma_g\ EXP\left(C_3\left(\frac{API}{T+460}\right)\right)}\right]^{1/C_2}, \quad \text{.....(A.31)}$$

Where the coefficients C_1, C_2, and C_3 are presented in **Table A1**;

Table A1 – Coefficients for Bubble Point Pressure in Vasquez and Beggs Correlation

Coefficient	API <= 30	API > 30
C_1	0.0362	0.0178
C_2	1.0937	1.1870
C_3	25.7240	23.9310

And the solution gas-oil ratio is expressed as;

$$R_s = C_1\,\gamma_g\,P^{C_2}EXP\left(C_3\left(\frac{API}{T+460}\right)\right), \quad \text{.....(A.32)}$$

The coefficients C_1, C_2, and C_3 are the same as for the bubble point pressure equation.

Oil formation volume factor for saturated oil is presented as;

$$B_o = 1 + C_1R_s + C_2(T-60)\left(\frac{API}{\gamma_g}\right) + C_3R_s(T-60)\left(\frac{API}{\gamma_g}\right), \quad \text{.....(A.33)}$$

Where the coefficients C_1, C_2, and C_3 are presented in **Table A2**;

Table A2 - Coefficients for Oil Formation Volume Factor in Vasquez and Beggs Correlation

Coefficient	API <= 30	API > 30
C_1	4.677×10^{-4}	4.670×10^{-4}
C_2	1.751×10^{-5}	1.100×10^{-5}
C_3	-1.811×10^{-8}	1.377×10^{-9}

For unsaturated oil;

$$B_o = B_{ob}\ EXP\big(c_o(P_b - P)\big), \quad \text{.....(A.34)}$$

Where oil compressibility, c_o, is expressed as;

$$c_o = \frac{A_1 + A_2 R_s + A_3 T + A_4 \gamma_g + A_5 API}{A_6 P}, \quad \text{.....(A.35)}$$

Where the coefficients A_1 through A_6 are presented in **Table A3**;

Table A3 - Coefficients for Oil Compressibility in Vasquez and Beggs Correlation

A_1	A_2	A_3	A_4	A_5	A_6
-1433.0	5.0	17.2	-1180.0	12.61	105

Note that, the temperature values, T, used in all equations should be in ^oF.

A.7 Velarde et al. Correlations

The Velarde *et al*. (1999) correlations contain equations for estimating bubble point pressure, solution gas-oil ratio, and oil formation volume factor. The correlation for the solution gas-oil ratio uses a reduced variable approach, and so the final equation is solved for the reduced solution gas-oil ratio. The reduced solution gas-oil ratio is defined as the solution gas-oil ratio divided by the solution gas-oil ratio at the bubble point. Similarly, the reduced pressure is defined as the pressure divided by the bubble point pressure.

$$P_r = \frac{P}{P_b}, \quad \text{.....(A.36)}$$

$$R_{sr} = \frac{R_s}{R_{sb}}, \quad \text{.....(A.37)}$$

The bubble point pressure is defined as;

$$P_b = 1091.47\left[R_{sb}^{0.081465}\gamma_g^{-0.161488}10^{X} - 0.740152\right]^{5.35489}, \quad \text{.....(A.38)}$$

Where;

$$X = (0.013098\,T^{0.282372}) - (8.2 \times 10^{-6} API^{2.176124}), \quad \text{.....(A.39)}$$

The solution gas-oil ratio at the bubble point pressure is expressed as;

$$R_s = \left[\frac{\left(\frac{P_b}{1091.47}\right)^{\frac{1}{5.35489}} + 0.740152}{\gamma_g^{-0.161488}\, 10^X}\right]^{\frac{1}{0.081465}}, \quad \text{.....(A.40)}$$

Where X is calculated the same as for the bubble point.

Once the reduced solution gas-oil ratio is calculated, the solution gas-oil ratio at the bubble point calculated above is used to solve for the solution gas-oil ratio at any pressure below the bubble point as;

$$R_{sr} = \alpha_1 P_r^{\alpha_2} + (1 - \alpha_1) P_r^{\alpha_3}, \quad \text{.....(A.41)}$$

Where;

$$\alpha_1 = A_0 {\gamma_g}^{A_1} API^{A_2} T^{A_3} {P_b}^{A_4}$$

$$\alpha_2 = B_0 {\gamma_g}^{B_1} API^{B_2} T^{B_3} {P_b}^{B_4}$$

$$\alpha_3 = C_0 {\gamma_g}^{C_1} API^{C_2} T^{C_3} {P_b}^{C_4}$$

The coefficients are presented in **Table A4** as;

Table A4 - Coefficients for Oil Solution Gas in Velarde *et al*. Correlation

$A_0 = 9.73 \times 10^{-7}$	$A_1 = 1.672608$	$A_2 = 0.929870$	$A_3 = 0.247235$	$A_4 = 1.056052$
$B_0 = 0.022339$	$B_1 = 1.004750$	$B_3 = 0.337711$	$B_3 = 0.132795$	$B_4 = 0.302065$
$C_0 = 0.725167$	$C_1 = 1.485480$	$C_3 = 0.164741$	$C_3 = 0.091330$	$C_4 = 0.047094$

And oil formation volume factor for saturated oil is presented as;

$$B_o = \frac{\rho_{STO} + 0.01357\ R_s\ \gamma_g}{\rho_{oR}}, \quad \text{.....(A.42)}$$

Where;

$$\rho_{oR} = \rho_{bs} - (0.00302 + 1.505\ {\rho_{bs}}^{-.951})(T - 60)^{0.938} +$$

$$(0.0233\ \times 10^{-0.0161\ \rho_{bs}})(T - 60)^{0.475}, \quad \text{.....(A.43)}$$

And,

$$\rho_{bs} = \rho_{po} + (0.167 + 16.181\ \times 10^{-0.042\ \rho_{po}})\left(\frac{P}{1000}\right) -$$

$$0.01(0.299 + 263\ \times 10^{-0.0603\ \rho_{bpos}})\left(\frac{P}{1000}\right)^2, \quad \text{.....(A.44)}$$

And,

$$\rho_{po} = 52.8 - 0.01R_{sb}, \quad \text{.....(A.45)}$$

$$\rho_a = -49.8930 + 85.0149\ \gamma_g - 3.70373\gamma_g\rho_{po} +$$

$$0.047981\gamma_g{\rho_{po}}^2 + \left(2.98914\ \rho_{po} - 0.035688{\rho_{po}}^2\right), \quad \text{.....(A.46)}$$

$$\rho_{po} = \frac{R_s\gamma_g + 4600\gamma_o}{73.71 + \frac{R_s\gamma_g}{\rho_a}}, \quad \text{.....(A.47)}$$

For unsaturated oil;

$$B_o = B_{ob}\ EXP\big(c_o(P_b - P)\big), \quad \text{.....(A.48)}$$

The oil compressibility, c_o, used in **Eq. A.48**, is obtained from the Vasquez and Beggs correlation. Note that, the temperature values, T, used in all equations should be in ^{o}F.

APPENDIX B

Assume an undersaturated oil reservoir with an initial reservoir pressure of 3455 psig. The reservoir is approximately 50 ft thick with an unknown oil-water contact. The reservoir oil has a bubble point pressure of 3233 psig determined with an oil gravity of 23.8 ^{o}API, gas gravity of 0.64, and a solution gas-oil ratio of 390 SCF/STB. The last measured reservoir pressure was 3155 psig obtained in November 2001. The reservoir has been produced by one well, from September 2000 until September 2004.The long-term reservoir pressure is estimated to be 3328 psig under abandonment conditions.

APPENDIX C

The Recommended Practice 13D (2006) is used to model the frictional losses inside the tubular and annular regions. The applied methodology is described as follows;

For tubular cross sections, to compute the $f[\{q, d_i, L, \mu\}]_{frictional\ \ loss}$ the following steps and parameters are to be determined;

$$K_{pipe} = \frac{5.11 R_{600}}{1022^{n_{pipe}}}, \quad \text{.....(C.1)}$$

$$n_{pipe} = 3.32 Log\left(\frac{R_{600}}{R_{300}}\right), \quad \text{.....(C.2)}$$

$$v_p = \frac{0.408\ q}{d^2}, \quad \text{.....(C.3)}$$

$$N_{\mathrm{Re}} = \frac{928 \cdot \rho \cdot v_p \cdot d}{\mu_e}, \quad \text{.....(C.4)}$$

$$\mu_e = 100 k_p \left[\frac{96 v_p}{d_p}\right]^{n_p - 1} \left[\frac{3n_p + 1}{4n_p}\right]^{n_p}, \quad \text{.....(C.5)}$$

For laminar flow;

$$f_p = \frac{16}{N_{\mathrm{Re}}}, \quad \text{.....(C.6)}$$

And for turbulent flow;

$$f_p = \frac{a}{N_{\mathrm{Re}}{}^{b}}, \quad \text{.....(C.7)}$$

$$a = \frac{Log(n_p) + 3.93}{50}, \quad \text{.....(C.8)}$$

$$b = \frac{1.75 - Log(n_p)}{7}, \quad \text{.....(C.9)}$$

$$\left(\frac{dp}{dL}\right) = \frac{f_p \cdot \bar{v}^2 \cdot \rho}{25.8 \cdot d}, \quad \text{.....(C.10)}$$

For annular cross sections, to compute the $f[\{q, dp_i, dp_o, dc_i, L, \mu\}]_{frictional\ \ loss}$ the following steps and parameters are to be determined;

$$K_{annulus} = \frac{5.11 R_{100}}{170.2^{n_{annulus}}}, \quad \text{.....(C.11)}$$

$$n_{annulus} = 0.657 Log\left(\frac{R_{100}}{R_3}\right), \quad \text{.....(C.12)}$$

$$v_a = \frac{0.408\ q}{d_2{}^2 - d_1{}^2}, \quad \text{.....(C.13)}$$

$$N_{\mathrm{Re}} = \frac{928 \cdot \rho \cdot v_a \cdot (d_2 - d_1)}{\mu_e}, \quad \text{.....(C.14)}$$

$$\mu_e = 100k_a\left[\frac{144v_a}{d_2 - d_1}\right]^{n_a-1}\left[\frac{2n_a+1}{3n_a}\right]^{n_a}, \quad \text{.....(C.15)}$$

For laminar flow;

$$f_a = \frac{24}{N_{\mathrm{Re}}}, \quad \text{.....(C.16)}$$

And for turbulent;

$$f_a = \frac{a}{N_{\mathrm{Re}}{}^{b}}, \quad \text{.....(C.17)}$$

$$a = \frac{Log(n_a)+3.93}{50}, \quad \text{.....(C.18)}$$

$$b = \frac{1.75 - Log(n_a)}{7}, \quad \text{.....(C.19)}$$

$$\left(\frac{dp}{dL}\right) = \frac{f_a \cdot \bar{v}^2 \cdot \rho}{25.8 \cdot (d_2 - d_1)}, \quad \text{.....(C.20)}$$

The hydrostatic pressure function, $f[\{\rho, Z\}]_{hydrostatic}$, is defined as;

$$0.052 \times \rho \times Z, \quad \text{.....(C.21)}$$

Where, ρ is in ppg, and Z is the true vertical depth in ft.

VITA

Name:	Amir Saman Paknejad
Address:	3116 TAMU, College Station, Texas, 77843
Email Address:	amirsaman@tamu.edu
Education:	B.S., Petroleum Engineering, Petroleum University of Technology, Iran, 2003 M.S., Petroleum Engineering, Texas A&M University, 2005 Ph.D., Petroleum Engineering, Texas A&M University, 2009